Research Article
Liver transplantation

JOURNAL
OF HEPATOLOGY

Primary cilia as a targetable node between biliary injury, senescence and regeneration in liver transplantation

Authors

Hannah Esser, Alastair Morris Kilpatrick, Tak Yung Man, …, Stefan Schneeberger, Sofia Ferreira-Gonzalez, Stuart John Forbes

Correspondence

sofia.ferreira-gonzalez@ed.ac.uk (S. Ferreira-Gonzalez), stuart.forbes@ed.ac.uk (S.J. Forbes).

Graphical abstract

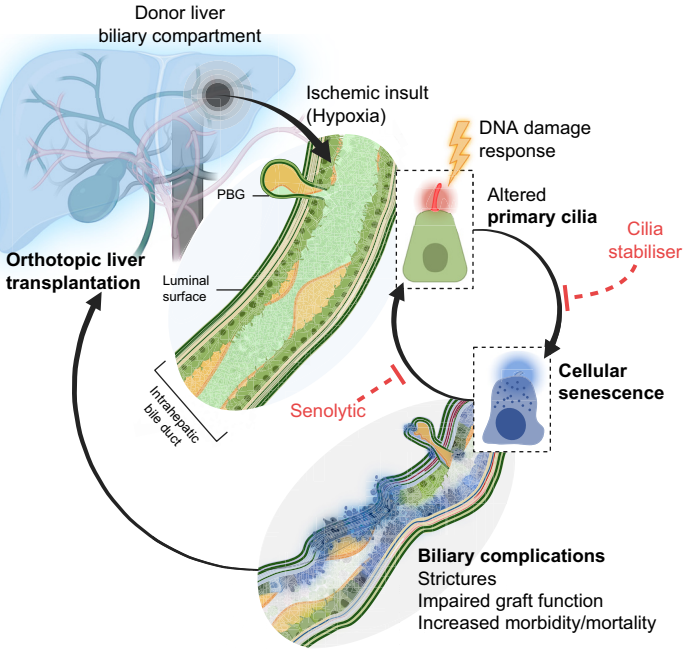

Highlights

- Liver pre-transplantation ischemic conditions damage the primary cilia (PC) of biliary epithelial cells (BEC).
- Elimination of PC induces cellular senescence in BEC.
- Senescent BEC cannot proliferate, leading to persistent biliary injury.
- Targeted PC interventions prevent biliary injury and promote regeneration.

Impact and implications

Up to 25% of liver transplants result in biliary complications, leading to additional surgery, retransplants, or death. We found that the incidence of biliary complications is increased by damage to the primary cilium, an antenna that protrudes from the cell and is key to regeneration. Here, we show that treatments that preserve the primary cilia during the transplant process provide a potential solution to reduce the rates of biliary complications.

https://doi.org/10.1016/j.jhep.2024.06.002
© 2024 The Authors. Published by Elsevier B.V. on behalf of European Association for the Study of the Liver. This is an open access article under the CC BY license (http://creativecommons.org/licenses/by/4.0/). J. Hepatol. 2024, 81, 1005–1022

Research Article
Liver transplantation

JOURNAL
OF HEPATOLOGY

Primary cilia as a targetable node between biliary injury, senescence and regeneration in liver transplantation

Hannah Esser[1,2,†], **Alastair Morris Kilpatrick**[1,†], Tak Yung Man[1], Rhona Aird[1], Daniel Rodrigo-Torres[1], Madita Lina Buch[1,2], Luke Boulter[3], Sarah Walmsley[4], Gabriel Corneliu Oniscu[5,6], Stefan Schneeberger[2], Sofia Ferreira-Gonzalez[1,4,*,‡], Stuart John Forbes[1,*,‡]

Journal of Hepatology **2024**. vol. 81 | 1005–1022

Check for updates

Background & Aims: Biliary complications are a major cause of morbidity and mortality in liver transplantation. Up to 25% of patients that develop biliary complications require additional surgical procedures, re-transplantation or die in the absence of a suitable regraft. Here, we investigate the role of the primary cilium, a highly specialised sensory organelle, in biliary injury leading to post-transplant biliary complications.

Methods: Human biopsies were used to study the structure and function of primary cilia in liver transplant recipients that develop biliary complications (n = 7) in comparison with recipients without biliary complications (n = 12). To study the biological effects of the primary cilia during transplantation, we generated murine models that recapitulate liver procurement and cold storage, and assessed the elimination of the primary cilia in biliary epithelial cells in the *K19CreER*^{T} *Kif3a*$^{fl/fl}$ mouse model. To explore the molecular mechanisms responsible for the observed phenotypes we used *in vitro* models of ischemia, cellular senescence and primary cilia ablation. Finally, we used pharmacological and genetic approaches to target cellular senescence and the primary cilia, both in mouse models and discarded human donor livers.

Results: Prolonged ischemic periods before transplantation result in ciliary shortening and cellular senescence, an irreversible cell cycle arrest that blocks regeneration. Our results indicate that primary cilia damage results in biliary injury and a loss of regenerative potential. Senescence negatively impacts primary cilia structure and triggers a negative feedback loop that further impairs regeneration. Finally, we explore how targeted interventions for cellular senescence and/or the stabilisation of the primary cilia improve biliary regeneration following ischemic injury.

Conclusions: Primary cilia play an essential role in biliary regeneration and we demonstrate that senolytics and cilia-stabilising treatments provide a potential therapeutic opportunity to reduce the rate of biliary complications and improve clinical outcomes in liver transplantation.

© 2024 The Authors. Published by Elsevier B.V. on behalf of European Association for the Study of the Liver. This is an open access article under the CC BY license (http://creativecommons.org/licenses/by/4.0/).

Introduction

Liver transplantation is the only curative option for many patients with end-stage liver disease. 35,000 liver transplants are performed annually worldwide, and the demand for healthy livers continues to increase, reflecting the international burden of chronic liver disease.[1] Unfortunately, 15-25% of liver transplant recipients develop post-operative biliary complications (BC), which continue to be a major cause of morbidity and mortality.[2–5]

BC encompass a plethora of conditions, including biliary leakage, anastomotic strictures (AS) and non-anastomotic strictures (NAS).[6] BC can have profound quality of life and economic implications:[7] both the readmission rate as well as the length-of-stay at the hospital double in case of BC. In an attempt to treat BC, patients undergo an average of 12 invasive procedures in the first 2 years after transplantation.[7] Unfortunately, BC – particularly NAS – are often refractory to treatment: in organs stemming from donation after cardiac death (DCD) BC results in a re-transplantation rate of 67%.[8]

Little is known about the causes of BC, and the gaps in our current knowledge impair the study of potential targets to reduce biliary injury and preserve bile duct function. Early rodent studies showing that bile ducts are highly susceptible to re-oxygenation following ischemia led to the postulation that the bile duct injury is most prevalent after transplantation.[9] However, a series of histological studies[10–12] reported that a high percentage of donor livers developed severe biliary epithelial loss during cold

* Corresponding authors. Address: MRC Centre for Regenerative Medicine, University of Edinburgh, 5 Little France Drive, Edinburgh, EH16 4UU, UK.
E-mail addresses: sofia.ferreira-gonzalez@ed.ac.uk (S. Ferreira-Gonzalez), stuart.forbes@ed.ac.uk (S.J. Forbes).
† Both authors contributed equally.
‡ Both authors contributed equally.
https://doi.org/10.1016/j.jhep.2024.06.002

storage, suggesting that the mechanisms underlying BC are already present before transplantation.

This phenotype has been attributed to toxic bile salt-induced injury,[13] prolonged donor warm ischemic time (WIT),[7] ischemia reperfusion injury (IRI)[12,14,15] and failure of the biliary epithelium to regenerate.[12,14–16]

Biliary regeneration is primarily driven by biliary epithelial cells (BEC): a heterogeneous, highly dynamic population of epithelial cells that possess primary cilia (*sing.* cilium, PC).[17,18] PC are highly specialised organelles that extend from the cell surface into the lumen, serving as bile flow-, chemo-, and osmo-sensors.[19–21]

PC are involved in BEC proliferation and biliary expansion following liver injury *in vivo*,[18,22–25] and are also required to maintain BEC viability *in vitro*.[22] The importance of PC in biliary regeneration is further illustrated by the occurrence of cholangiopathies[26] and developmental defects[27] in the absence of functional PC.

In this manuscript, we explore the effects of pre-transplantation conditions on PC structure and function and provide a comprehensive analysis of the role of this structure in biliary regeneration following ischemic injury.

We show that donor livers that post-operatively develop BC have shorter PC, with PC length inversely correlated with the duration of the ischemic period before transplantation. Damage to the PC during these ischemic conditions results in the establishment of cellular senescence, an irreversible cell cycle arrest that impairs regeneration, in BEC.

Our results suggest the presence of a negative feedback loop involving PC damage and cellular senescence that can be disrupted by targeted interventions to preserve PC structure and/or ablate cellular senescence, in order to preserve the regenerative capacities of the biliary tract and reduce biliary injury.

Finally, we show the clinical potential of this approach by perfusing human discarded donor livers with senolytics that target senescent cells and stabilise the PC, suggesting that interventions that focus on this organelle may help to reduce the burden of BC and improve outcomes in liver transplantation.

Material and methods

Clinical material

All human work was performed in accordance with the Data protection act 2018 and in accordance with the Caldicott principles-2018.

Human liver biopsies

Human liver protocol biopsies (n = 19) from transplanted livers were obtained from the Quality in Organ Donation national biobank (RAP 039). Needle biopsy peripheral liver samples from eight donation after brain death (DBD) and 11 DCD liver grafts were analysed. Donor data can be found in Table S1. Liver grafts were transplanted at the Scottish Liver Transplant Unit, Royal Infirmary of Edinburgh, and patient records were retrospectively screened for the development of post-operative BC as assessed by radiological pattern and clinical presentation. In total, seven recipients developed BC post liver transplantation (AS, n = 3; NAS, n = 4) (Table S2). Paraffin-embedded samples were anonymized, assessed histologically and later correlated with the clinical outcome.

Human livers

Ethical approval for the use of human livers declined for transplantation was received from the NHS Lothian research ethics committee reference number 15/SS/0218, NHS Lothian Research and Development (Project No. 2015/0408), and the NHS blood and transplant ethics committee (Research Innovation and Novel Technologies Advisory Group (registered as study 56)). Livers were retrieved by one of the National Organ Retrieval Teams (UK) and subsequently deemed unsuitable for transplantation by the responsible transplant surgeons. Livers were then offered to all UK liver transplant centres. If all centres declined the offer, livers were re-offered for research to registered studies. Donor data for included livers can be found in Table S3.

Human liver perfused with senolytics

Three liver grafts declined for transplantation were used for the senolytic flushing experiment (donor data can be found in Table S4). All grafts were initially preserved in Belzer MPS® Universal Wisconsin (UW) preservation solution (Bridge-to-life Ltd) at 4 °C. The left lateral segments (Couinaud Segments II and III) were dissected and prepared preserving the respective portal veins. One segment was flushed at 37 °C for 1 h with 1 L of sterile PBS (Sigma-Aldrich, D8537), supplemented with 5 mg/kg dasatinib (LC Laboratories, D-337) and 50 mg/kg quercetin (Sigma-Aldrich, Q4951) dissolved in 1 ml of DMSO (Thermo Scientific, 20688). The other segment (vehicle control) was flushed with PBS and DMSO.

Mouse models

Animals used in this study were C57BL/6 background, mix of males and females aged within 8–12 weeks at the start of the experiments. Mice were housed in a pathogen-free environment in open cages (NKP, M3-sloping front) at 21 °C with Aspen chips as bedding and kept under standard conditions with a 14-hour day cycle and access to food (irradiated RM3P) and water *ad libitum*. All animal experiments were carried out under procedural guidelines, severity protocols and with ethical permission from the Animal Welfare and Ethical Review Body (AWERB) and the Home Office (UK). All animal genotyping was outsourced commercially to Transnetyx, Inc (TN, USA) using the primers listed in Table S5.

Mouse model of liver procurement and static cold preservation

A mouse model of DBD and DCD-like liver procurement and subsequent cold storage (10 h) has previously been established in C57BL/6 mice aged within 8–12 weeks at the start of the experiments.[16] Briefly, for a DBD-like liver procurement animals were culled via cervical dislocation. Livers were procured and flushed with cold UW solution (Belzer MPS® UW solution (Bridge of Life)) via the portal vein. For DCD-like liver procurement, mice were exposed to increasing levels of CO_2 resulting in asphyxiation to model the agonal phase. Death of the mice was ensured by cervical dislocation. After 10 min of warm ischemia (asystolic phase) livers were procured and flushed with UW solution via the portal vein. Livers were then stored in a plastic bag with cold UW solution. The plastic bag was stored in another plastic bag filled with cold PBS and stored at 4 °C for 10 h.

p21$^{-/-}$ mice were a kind gift by Dr Tom Bird, Institute of Cancer Sciences, University of Glasgow, UK.

K19CreER^T Kif3a$^{fl/fl}$ for conditional primary cilia ablation
K19CreER^T+ and *K19CreER^T*– mice (in a C57BL/6 background) were crossed with Kif3a$^{fl/fl}$ mice to generate the *K19CreER^T Kif3a$^{fl/fl}$* line (Cre+ and Cre–). Mice were aged 8 to 12 weeks at the start of the experiments. Induction of animal models and recombination of loxP sites was achieved by three intraperitoneal applications of 4 mg tamoxifen (Sigma) dissolved in sunflower seed oil (Sigma) or sunflower seed oil only (control group). Long-term PC ablation in BEC was achieved by injecting 4 mg of tamoxifen every 15 days after the first induction protocol, for the duration of the experiment (6 months).

Dietary models of liver injury
3,5-diethoxycarbonyl-1,4-dihydrocollidine (DDC) diet was administered at 0.1% mixed with Rat & Mouse No.1 Maintenance diet (RM1, Special Diet Services) for up to two weeks. Methionine-choline deficient diet (MP Biomedicals) was administered for 2 weeks. Livers were collected following portal vein perfusion with PBS (Sigma-Aldrich, D8537). Organs were fixed in 10% formalin (VWR) for 12 h prior to embedding in paraffin blocks.

Mouse model of biliary senescence
K19CreER^T Mdm2$^{fl/fl}$ mice (in a C57BL/6 background) were used as previously published.[28] Briefly, upon Cre induction by tamoxifen via intraperitoneal injection, *Mdm2* is deleted in keratin 19 (K19)-positive BEC. As Mdm2 is a negative regulator of p53 its deletion results in overaccumulation of p53 which in turn leads to increased p21 expression.

Mouse model of senolytic/cilia stabiliser supplementation during liver procurement and static cold storage
Mouse livers were perfused with UW supplemented with either vehicle (DMSO (Thermo Scientific, 20688)), 15 μM ABT737 (ApexBio, A8193) or 10 μM Tubastatin A (TubA) (Sigma, SML0044) and then cold stored for 10 h in the same solution.

Mouse model of senolytic supplementation prior liver procurement
To assess the effect of senescence depletion prior cold storage, we administered 75 mg/kg ABT737 (SelleckChem) in 100 μl of vehicle solution: 10% Ethanol (Sigma-Aldrich), 30% PEG-400 (Sigma-Aldrich), 60% Phosal-50 (Lipoid AG). ABT737 was administered to C57BL/6 wild-type mice intraperitoneally for 7 consecutive days prior to liver procurement on cold storage (DBD-like liver procurement).

mBEC transplantation
Murine biliary epithelial cells (mBEC) isolated from *K19CreER^T Kif3a$^{fl/fl}$* mice were labelled with GFP using lentiviral transduction (plasmid pLenti-CMV-GFP-Puro; Addgene, #17448). GFP mBEC were treated *in vitro* with 5 μM 4-hydroxytamoxifen to induce primary cilia depletion or with vehicle solution (DMSO) for 2 h. mBEC were detached using accutase (StemPro^{TM}), washed in William's E medium and 1 x 10^6 GFP mBEC were resuspended for transplantation in 100 μl of sterile PBS. IRI was performed as previously described.[29] Briefly, under inhalatory anaesthesia a median laparotomy was performed and an atraumatic clip was placed on the portal vein. After 30 min of ischemia the clamp was removed and the spleen exposed to inject 1 x 10^6 GFP primary cilia competent or primary cilia deficient mBEC. Mice recovered in a heated cage at 30 °C and received post-operative analgesia (Carprofen, Pfizer) at 12 and 24 h. Blood samples were taken 24 and 48 h following surgery. Tissues were collected 48 h or 10 days following cell transplantation.

Tubastatin A treatment in IRI
WT mice were injected intraperitoneally with 10 mg/Kg of Tubastatin A prior to IRI. IRI was performed as stated above and blood samples were collected at 24 and 48 h after the ischemic insult. Tissues were collected at 48 h after the surgery.

Isolation of biliary tract areas
Intrahepatic bile ducts (IHBDs) were isolated as previously described.[16] Extrahepatic bile ducts (EHBDs) and gallbladder (GB) were collected using micro-forceps (FST) and micro-scissors (Moria) and processed to obtain RNA.

Cell culture

hBEC
Human BEC (hBEC) were isolated from discarded human donor livers and cultured as three-dimensional organoids as previously described.[30] Briefly, liver samples were mechanically digested and transferred into gentleMACS C-tubes (Miltenyi Biotec) with 15 ml of Hank's Balanced Salt Solution (Sigma-Aldrich) and 1.2 Wünsch units of liberase (Roche) for further 1.5 h digestion at 37 °C on the GentleMACS Octo Dissociator (Miltenyi Biotec). Samples were then passed through a 70 μm cell strainer (Corning) and sorted using CliniMACS CD133 magnetic beads (Miltenyi Biotec) to select the target CD133 positive hBEC population. EpCAM+ CD24+ CD31- CD45- CD133+ biliary phenotype was confirmed using FACS-sorting. Isolated hBEC were cultured as 3D organoids in Matrigel (Corning) with the expansion media described in Table S6. All experiments were performed between passages 3-10.

mBEC
To establish the mBEC culture, murine bile ducts were isolated from WT or *K19CreER^T Kif3a$^{fl/fl}$* mice as previously described.[16] Briefly, livers were dissected to approximately 2-4 mm^3 portions and digested using a mix of 0.125 mg/ml collagenase (Sigma-Aldrich, C9407) and 0.125 mg/ml dispase (Thermo Fisher, 17105-041) in 2% FCS Advanced DMEM/F-12 (Thermo Fisher). This mix was incubated 1 h at 37 °C. Bile ducts were identified under the microscope, individually collected, plated in Matrigel (Corning) and cultured for 7 days using the media stated in Table S7. Once the cultured was established as 3D organoids (4-5 passages) organoids were manually disrupted using a p200 pipette and cultured as 2D mBEC on collagen (Sigma-Aldrich, C3867) with the expansion media stated in Table S8. All experiments were performed at passage 12-20.

Primary cilia ablation in mBEC
2D mBEC culture was established from the bile ducts isolated from the *K19CreER^T Kif3a$^{fl/fl}$* model. To increase ciliation prior to the ablation assay, we used a modified serum starvation protocol:[31] mBEC medium was changed to William's E medium supplemented with Penicillin and Streptomycin for 12 h. To promote primary cilia ablation, mBEC were then incubated

for 2 h with 5 μM 4-hydroxy tamoxifen (Sigma-Aldrich, H7904) dissolved in methanol (VWR).

mBEC hypoxia assay
mBEC or hBEC were maintained at 37 °C for 6 h and 12 h in expansion medium in hypoxia (0.5% O_2, 5% CO_2, using a tri-gas incubator [NuAire]) or normoxia conditions (20% O_2, 5% CO_2).

EdU proliferation assay
3 μg/ml of 5-ethynyl-2'-deoxyuridine incorporation (EdU, Invitrogen, 11590926) were added to mBEC for the duration of the hypoxia/normoxia or 4-hydroxytamoxifen treatment.

mBEC induction of cellular senescence
mBEC were treated with 5 ng/ml recombinant murine transforming growth factor β (TGFβ, R&D, 7666-MB-005/CF) for 24 h as previously described.[32,33]

IMR90 induction of cellular senescence
IMR90 cells infected with an 4-hydroxytamoxifen inducible ER:RAS construct (IRAS) or a vector control (ISTOP) were kindly donated by Dr Juan-Carlos Acosta and cultured as previously described.[34] Briefly, 100 nM of 4-hydroxytamoxifen (Sigma-Aldrich, H7904) dissolved in DMSO (Thermo Fisher, 20688) was administered to the cells for senescence induction.

mBEC motility/migration studies
K19CreER^T Kif3a$^{fl/fl}$ mBEC grown in 2D were pre-treated for 2 h with 5 μM 4-hydroxy tamoxifen (Sigma-Aldrich, H7904) dissolved in methanol (VWR) to induce PC ablation. Control cells (PC competent) were treated only with methanol. Cells were then placed in the Opera Phoenix Plus High-Content Screening System (PerkinElmer, HH14001000) and 20 ng/ml of mouse hepatocyte growth factor (Peprotech) added to induce cell motility.[35] Cells were imaged over 12 h with a total of 194 timepoints.

Rhodamine 123 transport assay
Organoids grown from isolated bile ducts were incubated with 100 μM of Rhodamine 123 (Sigma-Aldrich) for 5 min at 37 °C, washed 3 times with media and then kept in fresh media for 1 h. After 1 h, multiple fluorescence measurements were performed between the organoid lumen and the surrounding background. Rhodamine 123 fluorescence in the organoid lumen was normalised over the background measured in the surrounding areas and expressed as fluorescence units.

Imaging

Histology
3D BEC were encapsulated in the well using 2% Agarose (Sigma-Aldrich) dissolved in PBS (Sigma Aldrich, P4417-100TAB). Agarose capsules were fixed overnight with formalin and transferred to paraffin blocks for subsequent processing. 2D BEC were fixed in cold methanol:acetone (1:1) (Fisher Chemical) for 10 min and washed with PBS before staining. EdU stained BEC were treated with 2N HCl (Sigma-Aldrich) for 30 min at room temperature prior staining. For tissue, 4 μm paraffin sections were dewaxed, rehydrated and antigen retrieval was achieved with 100 mM Sodium Citrate pH 6.0 or 100 mM Tris-EDTA pH 9.0 at high power in a microwave for 10-15 min.

Immunofluorescence
Tissue sections/3D BEC/2D BEC were treated for 30 min with protein block (Spring Bioscience) at room temperature and incubated with the primary antibodies listed in Table S9. Primary antibodies were detected using fluorescent conjugated secondary antibodies (Alexa-488, 555 or 647, Invitrogen). Sections were incubated with DAPI (Sigma-Aldrich) and mounted with Fluoromount-G (SouthernBiotech). Isotype controls were used at the same concentration as the corresponding primary antibodies.

Immunohistochemistry
Tissue sections were blocked for endogenous peroxidase and alkaline phosphatase activity (Bloxall, Vector), endogenous avidin/biotin expression (Invitrogen) and nonspecific protein binding (Spring Bioscience). Sections were incubated with the primary antibodies listed in Table S9. Species-specific secondary biotinylated antibodies (Vector), Vectastain R.T.U, ABC reagent (Vector) and DAB chromogen (Dako) were used sequentially to detect the primary antibody. Sections were counterstained with haematoxylin.

SA-β-galactosidase (SA-β-Gal) assay was performed using commercial kit #9860 from Cell Signaling according to the manufacturer's instructions.

Image acquisition
Images were acquired using a Leica TCS SP8 (Leica), Nikon A1-R HD25 (Nikon), Operetta CLS High-Content Analysis System (PerkinElmer, HH16000000), Opera Phenix Plus High-Content Screening System (PerkinElmer, HH14001000), Vectra Polaris (Akoya) or Nikon Eclipse e600 microscope (Nikon), NIS-Elements Confocal (Nikon). Images were acquired in up to four fluorescent channels at up to 63X magnification. DAPI, Alexa Fluor 488, 555 and 647 were detected using band paths of 415-480, 495-540 and 594-633 lasers respectively. 3D mBEC were imaged using the iRiS^{TM} Digital Cell Imaging System (PerkinElmer). Confocal images were deconvolved using the Huygens Professional Software (SVI) to enhance resolution.

Image analysis
Histological sections were assigned a randomized blinded code prior to imaging by a separate researcher and the randomization decoded at the time of the final data analysis. Images were then analysed using different software systems such as Fiji ImageJ,[36] Columbus Image Analysis Software (2.9.1.532 PerkinElmer) and inForm Image Analysis Software (version 2.3, PerkinElmer/Akoya). Videos were edited using Filmora video editor.

Primary cilia length analysis
2D cells and tissue sections were stained for DAPI and acetylated α-tubulin[17] or ARL13B.[37] Sections were then imaged using Leica TCS SP8 (Leica) or Nikon A1-R HD25 (Nikon), deconvolved using Huygens Professional Software (SVI) and analysed using Fiji ImageJ software. Primary cilia length was determined by first creating a z-stack maximal projection image (based on maximal intensity) and subsequently using the

freehand line tool to measure length. In case of a liver tissue section, all clearly identifiable cilia in each bile duct lumen as well as bile duct diameter were measured. Quantification cilia length and number of ciliated cells was performed manually on 10 random non-overlapping fields per section (x63 magnification).

EdU, 53BP1 and γH2A.X analysis
Stained cells were imaged and analysed using the Columbus software (2.9.1.532 PerkinElmer). For each experiment identical thresholds were used in all images for assigning nuclei to a specific population.

Senescence markers analysis
Stained cells were imaged using the Vectra Polaris system (Akoya), the Operetta CLS High-Content Analysis System (PerkinElmer, HH16000000) or the Opera Phenix Plus High-Content Screening System (PerkinElmer, HH14001000). Images were analysed using the inForm image analysis software (Akoya), Columbus software (2.9.1.532 PerkinElmer) or Signals Image Artist software (PerkinElmer, 1.0) depending on the equipment used. Cells were segmented based on nuclear (DAPI +/- senescence or proliferation marker) and cytoplasmic (K19) stains. Cells were then categorized into marker positive or negative based on nuclear positivity for the stained marker. For each experiment identical thresholds were used in all images for assigning nuclei to a specific population.

SA-β-Gal analysis
SA-β-Gal, K19 and DAPI stained slides were scanned. Using the Columbus/Signals Image Artist software cells were identified using nuclear (DAPI) and cytoplasmic staining (K19). Using the software's linear classifier system, an algorithm to identify SA-β-Gal-positive cells was established and trained. Cells were classified into SA-β-Gal-positive and SA-β-Gal-negative cells.

Molecular biology

RNA isolation, RT-qPCR and gene expression analysis
RNA was isolated and purified using RNeasy RNA extraction kit (Qiagen) according to the manufacturer's instructions. RNA concentration and quality was assessed using a Nanodrop ND-1000 spectrophotometer (Thermo Fisher). Reverse transcription was performed using QuantiTect Reverse transcription kit (Qiagen). Real time-qPCR was performed on a LightCycler 480 II (Roche) with commercial primers from Qiagen's QuantiTect (stated in Table S10). Each gene expression was assessed with its own standard curve and normalised to a housekeeping gene (*ACTB2, Actb2* and *Gapdh*). Samples were run in duplicates.

qPCR arrays
400 ng of total RNA were reverse transcribed using the RT^2 First Strand Kit (Qiagen) following the manufacturer's protocol. The cDNA was then diluted with nuclease-free water and added to the RT^2 SYBR Green qPCR Mastermix (Qiagen). 10 μl of the cDNA -SYBR Green mix was added to each well of the human RT^2 Profiler^{TM} PCR Array Human Primary Cilia (Qiagen) or the RT^2 Profiler^{TM} PCR Array Mouse Hypoxia Signaling Pathway (Qiagen). Real-Time PCR was performed on the Roche LightCycler 480 II (Roche) and used SYBR green detection. All data from the PCR was collected by the LightCycler Software 4.1 (Roche Life Science). Fold change and *p* values were computed for each gene based on gene expression as determined by PCR array. Average group expression for each gene was computed by harmonic mean over replicates. Normalised gene expression was defined as 2-ΔCt, where ΔCt is the average group expression for each gene, subtracting the average group expression for the chosen housekeeping genes, which were chosen for each array by the RT2 Profiler PCR Array data analysis software (GeneGlobe; Qiagen). Data was imported into R, then fold change was computed for each gene as the ratio of normalised gene expression in the test and control groups. Normalised gene expression was then calculated similarly for each replicate. *p*-values were computed for each gene using a two-tailed Student's *t* test of the normalised replicate gene expression values in the test vs the control groups; significant genes were defined as $p \leq 0.05$. Heatmaps were generated with the heatmap R package and show significantly differentially expressed genes. Data represents normalised gene expression for each replicate, centred and row-scaled. Genes are ordered based on hierarchical clustering.

RNA sequencing
500 ng of total-RNA sample was used for RNA-seq library preparation, using the NEBNext Ultra II Directional RNA Library Prep Kit (NEB #7760) and the Poly(A) mRNA magnetic isolation module (NEB #E7490) according to the manufacturer's protocol. AMPure XP beads (Beckman Coulter #A63881) were used to purify the cDNA library. Multiple indexing adapters were ligated to the ends of the ds cDNA to prepare them for hybridisation onto a flow cell, before 10 cycles of PCR were used to selectively enrich those DNA fragments that had adapter molecules on both ends and amplify the amount of DNA in the library suitable for sequencing. Following amplification, libraries were purified using AMPure XP beads. Completed libraries were quantified by fluorometry using the Qubit dsDNA HS assay and assessed for quality and fragment size using the Agilent Bioanalyser with the DNA HS Kit (#5067-4626). Fragment size and quantity measurements were used to calculate molarity for each library pool. Sequencing was performed on the NextSeq 2000 platform (Illumina Inc, #20038897) at the Edinburgh Clinical Research Facility, Western General Hospital, Edinburgh, UK, using NextSeq 1000/2000 P2 Reagents (200 Cycles) v3 (#20046812). Libraries were combined in an equimolar pool based on Qubit and Bioanalyser assay results and run over a single P2 flow cell.

RNA-seq analysis
Read quality of sequenced FASTQ files was assessed using FastQC and MultiQC (v.1.3.dev0).[38] Adapter sequences, poly-G sequences and low-quality bases (Phred <20) were trimmed using Cutadapt (v.1.16);[39] subsequent quality assessment confirmed adapter contamination of <0.1% per sample. Reads were aligned to the mouse reference genome (GRCm38.100) with STAR (v.2.7.1a).[40] Data was imported into R and reads counted using the featureCounts function from the Rsubread Bioconductor package (v.2.0.1);[41] genes with no symbol were excluded from downstream analysis. Differential expression was computed using DESeq2 (v.1.34.0).[42] For heatmap visualisation of RNA-seq data, read counts were normalised with respect to library size using the regularized log (rlog) transform.[42] Cilia-associated genes were extracted from the syscilia

Gold Standard database (v1).[43] Additional data mining of Gene Ontology terms was carried out via AmiGO 2.[44]

The RNA-seq data associated with this study has been deposited in NCBI Gene Expression Omnibus (SuperSeries accession number GSE220722).

scRNA-seq analysis

Pre-processed single-cell RNA sequencing (scRNA-seq) data generated using the Smart-Seq2 protocol was downloaded from Gene Expression Omnibus (GSE115301;[45]). FPKM expression data for 224 IMR90 cells (100 growing cells, 41 Day 2 cells, 42 Day 4 cells and 41 senescent cells) was used to visualise expression of senescence-related genes and cilia-related genes as above. Genes identified as being significantly differentially expressed between growing and senescence conditions (false discovery rate <0.05) were queried to identify significantly differentially expressed cilia-related genes.

We also queried a published meta-analysis of senescent fibroblast transcriptomic datasets independent of senescence stimulus. Hernandez-Segura et al. published a meta-analysis of senescent fibroblast transcriptomic datasets and identified a number of genes differentially expressed by senescent fibro blasts, regardless of the senescence stimulus 1,311 of which were not shared with quiescent cells, a reversible cell cycle arrest different from cellular senescence.[46]

We used these genes to identify genes that were also cilia-associated, based on their presence in the syscilia Gold Standard database.[43,47] The identified cilia-associated genes are shown ranked by fold change, computed using a negative binomial generalized linear model (NB-GLM).

Publicly available scRNA-seq data deriving from primary tissue from intrahepatic bile ducts was downloaded from ArrayExpress (E-MTAB-8495).[48] Demultiplexing of scRNA-seq data, alignment and barcode counting were performed using 10x Genomics Cell Ranger (v5.0.0) with reference dataset GRCh38/2020-A. Unfiltered UMI count matrices from Cell Ranger were used as input for downstream analysis with the Seurat R package (v4.4).[49] Cells were filtered to remove those with <200 features. Features present in <3 cells were removed. BEC were then isolated following the method of Sampaziotis *et al.*,[48] where cells with >3 counts for at least one of the human biliary markers (EpCAM, keratin 7 and K19) were retained for downstream analysis; samples with fewer than 50 retained cells were removed from analysis. Cells were classified as EpCAM+, EpCAM+CD133+, or EpCAM+CD133- based on detectable expression of these genes. scRNA-seq expression density plots were visualised using the Nebulosa R package (v1.8).[50]

Western blot

Whole cells were lysed with RIPA Buffer (Thermo Scientific; 89900) and Halt™ Protease Inhibitor Cocktail (100x) (Thermo Scientific; 78430) at 4 °C for 30 min. The lysate was spun for 5 min at 21,000 rcf. The supernatant was taken and incubated with loading dye (Invitrogen NuPage LDS Sample Buffer (4x); 2083421) for 10 min at 95 °C. Protein lysates as well as ladder (Novex Sharp Pre-Stained; LC5800) were then transferred on 4–12% Bis–Tris Polyacrylamide gels (Invitrogen) according to the manufacturer's instructions using MOPS buffer (Novex NuPage MOPS SDS Running Buffer 20x; NP0001). Proteins were transferred onto 0.45 μm nitrocellulose membrane (Amersham, Protran XL), blocked in 3.5% skimmed milk and stained with primary antibody as stated in Table S11 diluted in blocking solution at 4 °C overnight, washed and incubated with Li-COR fluorescent conjugated secondary antibodies (anti-mouse 800CW 925-32212, anti-rabbit 680RD 926-68073) diluted 1:10,000 for 1 h at room temperature. Images were acquired and analysed using a Li-COR Odyssey XF imager (Li-COR). Signal intensity of each band was evaluated as measured by Image Studio Lite (version 5.2.5, Li-COR). Membranes were treated with 30% H_2O_2 for 15 min at room temperature prior to re-probing (blocking, primary antibody, secondary antibody).

All original uncropped western blots can be found in Fig. S19.

Statistical analysis

Prism software version 9 (GraphPad Software, Inc) and R (RStudio) were used for statistical analysis. For parametric data, statistical significance was computed using a two-tailed unpaired Student's *t* test. Non-parametric data was tested for statistical significance using a Mann-Whitney *U* test. In cases where more than two groups were being compared, a one-way ANOVA (with Bonferroni correction) was used. Fisher's exact test was used for analysis of contingency tables. Statistical significance was assumed at p <0.05. Data is presented as mean ± SEM. n refers to biological replicates.

Routinely qPCR experiments were performed in technical triplicates of multiple biological replicates. For representative images 3-4 liver lobes were examined histologically in at least 3 biological replicates; further details referring to the specific numbers of biological replicates for each experiment can be found in the respective figure legends.

Results

PC shortening is associated with the development of BC post liver transplantation

Liver grafts for transplantation can be procured from living or, predominantly, from deceased donors following diagnosis and confirmation of death using cardio-respiratory (DCD) or neurological criteria (DBD)[51] (Fig. 1A).

Both DCD and DBD liver grafts are exposed to ischemic periods prior to transplantation: cold ischemic time (CIT) is defined as the interval from initiation of cold organ preservation to reperfusion of the liver.[52] DCD donor livers undergo an additional period of WIT from withdrawal of life support to cold storage, characterised by reduced blood supply[53] (Fig. 1A).

In homeostasis, PC can be found in the lumen of bile ducts,[26] as small sensory organelles protruding from the BEC surface (Fig. 1B). To address the physiological effects of ischemia in PC during DBD and DCD procurements, PC length was assessed in human liver protocol biopsies taken after liver procurement and prior to cold storage (donor characteristics and type of BC are summarised in Table S1 and Table S2, respectively).

Liver grafts that later develop BC displayed significantly shorter PC, in comparison with those that did not develop BC (Fig. 1C). As PC length correlates with bile duct size,[26] we also assessed bile duct diameter but found no significant difference between BC and non-BC groups (Fig. 1C). This suggests that

the structure of PC on BEC is already compromised prior to transplantation.

Next, we correlated PC length with the type of donor procurement and ischemic times in livers declined for transplantation (Table S3). Increasing CIT, in both DBD and DCD liver grafts, results in significantly decreased PC length (Fig. 1D), with DCD grafts displaying shorter PC in comparison with CIT-matched DBD grafts (Fig. 1E). These results suggest that the period of WIT during DCD procurement exacerbates the shortening of PC in BEC, reinforcing clinical observations that suggest that prolonged WIT during procurement is associated with higher BC rates.[3]

As hypoxia is a key factor for ischemia during liver transplantation,[54,55] we exposed human BEC grown as 3D organoids to hypoxic conditions. Increasing the length of hypoxia exposure significantly altered the levels of hypoxia-associated genes *HIF1A*, *HIF2A*, *EGLN1*, and *EGLN3* (Fig. S1A),[56,57] and significantly decreased the overall volume of the

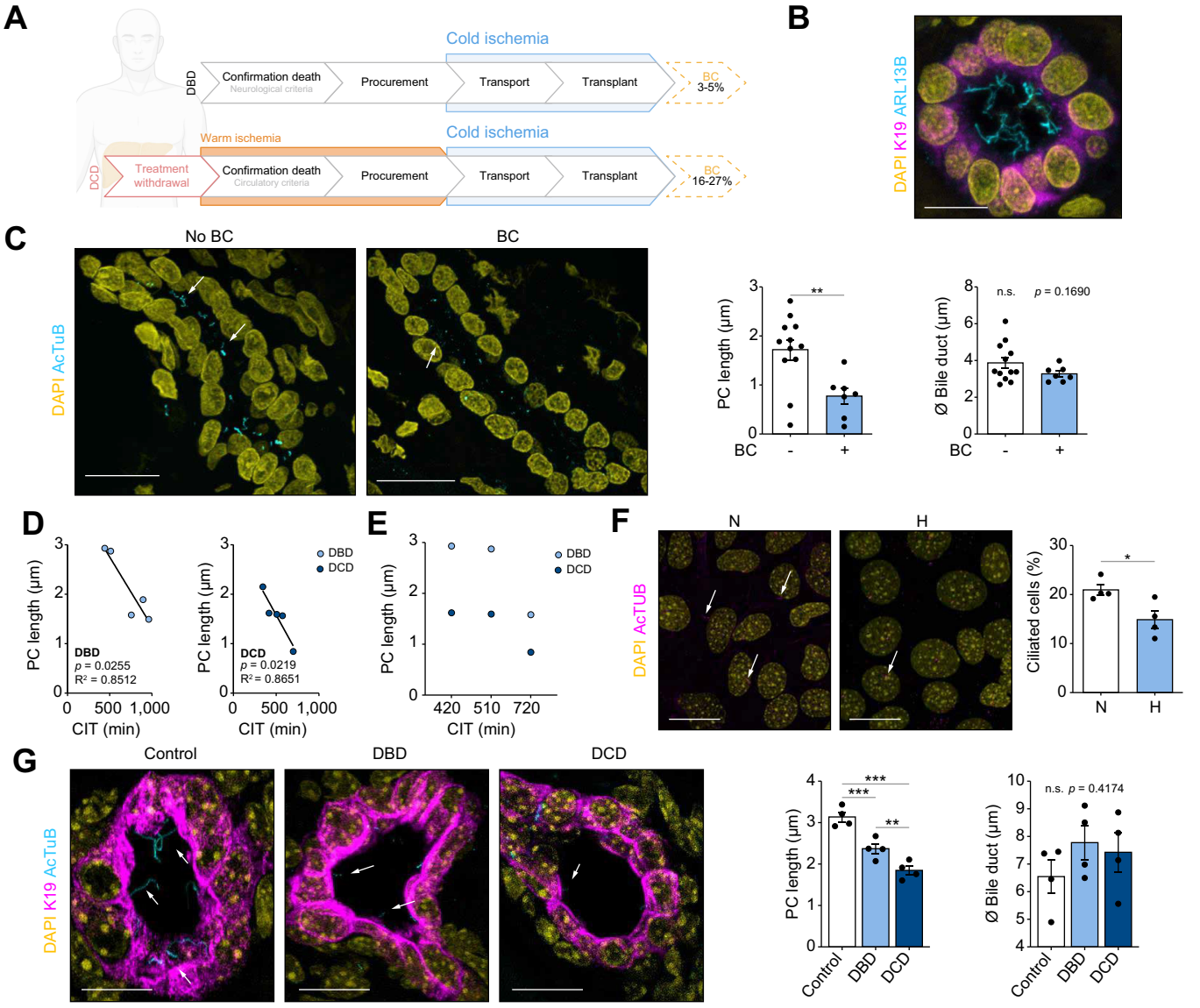

Fig. 1. PC length decreases in patients with post-operative BC. (A) Schematic representation of liver procurement in DBD and DCD (including a period of warm ischemia) donation. (B) Human bile duct immunofluorescence, depicting K19-positive BEC (magenta), ARL13B PC's axoneme (cyan), and DAPI (yellow). SB = 10 µm. (C) Representative images of PC (AcTub, cyan) in the intrahepatic bile ducts of human biopsies from a liver that did not develop BC (No BC) and a liver that developed BC. Presence of PC is indicated with white arrows. SB = 10 µm. Right, Quantification of PC length and bile duct diameter in the samples that developed BC (+, n = 12) and those that did not (-, n = 7). $^{**}p$ <0.01 (mean ± SEM); Student's *t* test. (D) Correlation of CIT with the PC length, for DBD (light blue) or DCD (dark blue) human livers declined for transplantation. Pearson correlation. (E) Correlation of DBD (light blue) and DCD (dark blue) liver grafts. DCD grafts display shorter PC than CIT-matched DBD liver grafts. (F) Immunofluorescence of PC (AcTub, magenta) in mouse BEC subjected to 6 h of normoxia (N, 20% O_2, 5% CO_2) or hypoxia (H, 0.5% O_2, 5% CO_2). White arrows indicate PC, SB = 10 µm. Right, percentage of ciliated BEC during normoxia (N, n = 4) or hypoxia (H, n = 4). $^{*}p$ <0.05 (mean ± SEM); Student's *t* test. (G) Immunofluorescence of mouse bile ducts (K19, magenta) and PC (AcTub, cyan) in mouse control (no cold storage, n = 4), DBD (+10 h of cold storage, n = 4), and DCD (+10 h of cold storage, n = 4). White arrows indicate PC, SB = 10 µm. Right, quantification of PC length and bile duct diameter. $^{***}p$ <0.001, $^{**}p$ <0.01 (Mean ± SEM); Student's *t* test. BC, biliary complications; BEC, biliary epithelial cells; CIT, cold ischemic time; DBD, donation after brain death; DCD, donation after cardiac death; H, hypoxia; N, normoxia; PC, primary cilia.

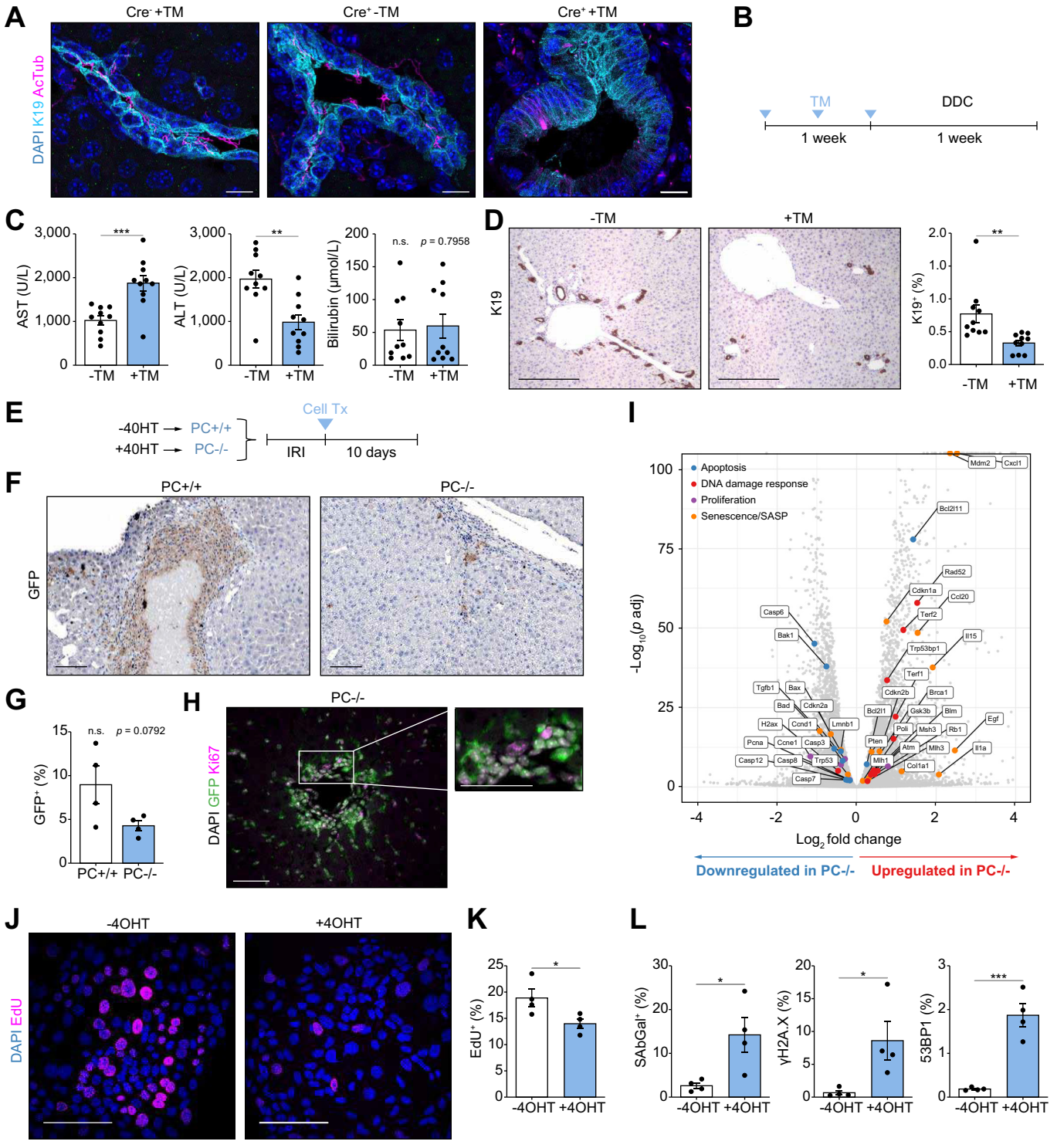

Fig. 2. *In vitro* and *in vivo* effects of PC loss in BEC. (A) Representative immunofluorescence of PC in the *K19-CreER*^{T} *Kif3a*$^{fl/fl}$ model. From left to right: TM administration in Cre- mice (negative control), vehicle (sunflower oil) in a Cre+ mouse, and TM in Cre+ mouse. DAPI depicts nuclei, K19 (Cyan) the BEC, and AcTub (magenta) the axoneme of the PC. n = 4 per group. SB = 12 μm. (B) Schematic representation of the model: PC was ablated via three intraperitoneal doses of TM on alternate days and mice were subjected to 1 week of DDC diet. (C) Liver function tests: AST, ALT, and bilirubin in uninduced (-TM) *vs.* induced (+TM) mice, following a week of DDC diet. ***p* <0.01, *** *p* <0.001 (Mean ± SEM); Student's *t* test, n = 10 per group. (D) K19 representative immunohistochemistry in uninduced (-TM) *vs.* induced (+TM) mice following elimination of the PC and a week of DDC diet. Right, percentage of K19+ per field of view. ***p* <0.01 (Mean ± SEM); Student's *t* test. n = 10 per group. SB= 120 μm. (E) Schematic representation of the model: mice were subjected to 30 min of hepatic IRI and immediately transplanted with GFP-positive BEC pre-treated with vehicle (-4OHT; PC competent, PC+/+) or 4OHT (+4OHT;PC depleted, PC-/-). (F) Representative GFP immunohistochemistry in both groups. n = 4 per group, SB = 120 μm. (G) Quantification of PC+/+ (PC competent) or PC-/- (PC depleted) GFP+BEC per field of view at 10 days after IRI. Student's *t* test, n = 4 per group. (H) Immunofluorescence of GFP and Ki67 in PC-/- (PC depleted) GFP-positive cells. SB = 50 μm. Far right, digital magnification depicting area of interest. (I) Volcano plot of genes significantly differentially expressed between PC-depleted (PC-/-; +4OHT treated) and PC-competent (PC+/+; -4OHT) BEC identified through RNA-seq

organoids (Fig. S1B), suggesting a strong hypoxic response and impaired organoid proliferation.

In vitro assessment of PC (Fig. S1C) suggests that murine BEC exposed to hypoxia (0.5% O_2, 5% CO_2) have fewer and shorter PC in comparison with BEC exposed to normoxia (20% O_2, 5% CO_2), as assessed by acetylated-α-tubulin (AcTub) immunofluorescence (Fig. 1F). This result is consistent with our observation of a significant decrease in the gene expression levels of *KIF3A* (a key factor responsible for PC structural maintenance) (Fig. S1D). We also found significant downregulation of genes vital for ciliary organisation and cilia maintenance after exposure to hypoxia, accompanied by an upregulation of *FOS*, known to be induced by hypoxia[58] (Fig. S1E).

To understand if these results represented a mechanism conserved between species, we generated a mouse model that simulates DBD and DCD procurement.[16] Briefly, the mouse liver is perfused *in situ* with UW preservation solution, removed and submerged in UW in a cold receptacle (4 °C) for 10 h of CIT. For DBD-like procurement, mice were euthanised via cervical dislocation. For DCD procurement, mice were exposed to increasing levels of CO_2 (resulting in asphyxiation to model the agonal phase of procurement), followed by cervical dislocation and 10 min of WIT (asystolic phase). We also included a control group with no cold storage (0 h CIT) following DBD-like procurement.[16]

Our immunohistochemistry assessment indicates that, in comparison with control bile ducts, both DBD and DCD livers have significantly shorter PC after 10 h of CIT. DCD bile ducts were the most significantly affected group (Fig. 1G). No significant differences in bile duct diameters between all the groups were observed ($p = 0.4174$) (Fig. 1G).

Altogether, our data suggest that CIT and WIT affect the PC structure during liver procurement, and that these structural changes are correlated with BC during post-transplantation stages.

To understand if the observed PC alterations can be used as a predictive factor for the presence of AS or NAS development, we have studied donor and recipient data with the following results:

- For the grafts transplanted in these patients, we found no significant differences in donor age or transaminases between healthy, AS and NAS groups (Fig. S2A,B).
- Direct comparisons of PC length with donor transaminases (assessed during procurement) or recipient transaminases (assessed at 12 months after transplantation) display no significant correlation (Fig. S2C). Similarly, no significant correlations were found between PC length and donor age (Fig. S2D); or between PC length and donor BMI (Fig. S2E).
- Bile duct diameter was similar for the three groups (Fig. S2F), suggesting that any potential differences in PC length were not associated with intrahepatic duct size.
- No significant differences in PC length were found between AS and NAS groups (Fig. S2G).

AS and NAS develop in different regions of the biliary tract (intrahepatic and extrahepatic areas, respectively). As differences in PC length per biliary areas have been previously reported[17] (Fig. S3A.1-2), we also explored PC regional variability in the human biliary tract using the publicly available scRNA-seq data from Sampaziotis and colleagues.[48] In our re-analysis of this data, we studied the expression patterns of ciliary markers in BEC isolated from three different regions: IHBD, EHBD and GB (Fig. S3B).

We found a similar pattern of expression for genes associated with PC structure and maintenance (*e.g.*, *KIF3A*, *ARL13B*, *AHI1* and *IFT88*) in all regions (Fig. S3C).

However, genes associated with cilia function display region-specific variation in their expression. For example: genes associated with Hedgehog and Hippo pathways (*PTCH1*, *SUFU*, *RGRIP1L*, and *LATS1/2* and *MST1* respectively) have a higher overall expression in IHBD areas (Fig. S3D-E), whereas Wnt-related genes (*FZD1*, *INVS*, *NPHP3*) are present in IHBD, EHBD and GB (Fig. S3F). Notch-related genes (*NOTCH3*, *PSEN1*) show wide region-specific variability (Fig. S3G) and *TGFB1* appears to be specific to IHBD (Fig. S3H).

Altogether, these data suggest that although PC shortening is characteristic of BC in general, it cannot be used as a predictive factor to distinguish between AS and NAS.

Loss of PC induces BEC senescence *in vitro* and *in vivo*

To assess the effects of PC depletion in BC, we developed a model in which the PC are eliminated exclusively in BEC: tamoxifen-inducible *K19CreER^T Kif3a$^{fl/fl}$* mice.

Kif3a is part of the intraflagellar transport machinery required for ciliary assembly and trafficking of signaling pathway components,[59] and elimination of *Kif3a* results in PC ablation.[60,61] Therefore, BEC-specific deletion of *Kif3a* results in PC ablation in bile ducts (Fig. 2A). Next, to provoke a BEC response, we subjected the *K19CreER^T Kif3a$^{fl/fl}$* mouse to different dietary models of biliary disease.

First, we induced PC depletion using three doses of tamoxifen, before placing the animals on a DDC diet for 1 week. DDC diet induces sclerosing cholangitis, expansion of the biliary compartment (ductular reaction), and biliary fibrosis[62] (Fig. 2B). Analysis of transaminases indicates a significant increase in aspartate aminotransferase (AST) in the PC-depleted group, accompanied by a significant decrease in alanine aminotransferase (Fig. 2C). No significant changes were observed in bilirubin levels (Fig. 2C). PC ablation followed by 1 week of DDC diet results in a significantly reduced ductular reaction as assessed by H&E, Keratin 19 and EpCAM immunohistochemistry (Fig 2D and Fig. S4A-C). No significant changes in the levels of fibrosis were observed in the PC-depleted group, as assessed by Picrosirius Red staining (Fig. S4D).

This absence of ductular reaction is also observed when the PC-depleted group is placed on 2 weeks of DDC diet (Fig. S4E-H), or 2 weeks of methionine-choline deficient diet, a classical dietary model of non-alcoholic steatohepatitis[63] (Fig. S4I-L).

analysis. Highlighted genes are associated with apoptosis (blue), DNA damage response (red), proliferation (purple) and senescence/SASP (orange). (J) EdU immunofluorescence in -4OHT or +4OHT treated BEC *in vitro*. SB = 50 μm. n = 4 per group. (K) Percentage of EdU in -4OHT- or +4OHT-treated BEC *in vitro*. *p <0.05 (Mean ± SEM); Student's *t* test, n = 4 per group. (L) Percentage of SA-β-Gal, γH2A.X and 53BP1 in -4OHT- or +4OHT-treated BEC *in vitro*. *p <0.05, *** p <0.001 (Mean ± SEM); Student's *t* test, n = 4 per group. 4OHT, 4-hydroxytamoxifen; AcTub, acetylated-α-tubulin; ALT, alanine aminotransferase; AST, aspartate aminotransferase; BEC, biliary epithelial cells; DDC, 3,5-diethoxycarbonyl-1,4-dihydrocollidine; IRI, ischemia reperfusion injury; PC, primary cilia; SASP, senescence-associated secretory phenotype; SA-β-Gal, SA-β-galactosidase; TM, tamoxifen.

Together, these data suggest that ductular reaction in liver disease relies on the presence of a functional PC in BEC.

Long-term depletion of PC in BEC (Fig. S5A,B) results in a significant decrease of bilirubin, cholesterol, AST, alanine aminotransferase and albumin, alongside a significant increase in alkaline phosphatase (Fig. S5C). After 6 months we observed no ductular reaction (Fig. S5D,E), but noted the presence of biliary cysts (Fig. S5D-G), infiltration of inflammatory cells (Fig. S5G) and absence of fibrosis (Fig. S5H), indicating biliary tract-specific disruption and altered metabolic response.

To explore the mechanisms responsible for the absence of ductular reaction with PC ablation, we isolated the bile ducts from the *K19CreER^T Kif3a$^{fl/fl}$* mice and grew them as 3D organoids *in vitro* (Fig. S6A). Similar to the *in vivo* induction, we then added either 4-hydroxytamoxifen (4OHT) to the culture to ablate the PC, or DMSO as control. mBEC treated with 4OHT decrease their percentage of ciliation and show a decreasing trend in PC length (Fig. S6B,C). We also confirmed *Kif3a* floxing, as indicated by the overall decrease of KIF3A protein (Fig. S6D).

Upon PC depletion, 3D organoids alter their morphology, shrink and collapse (Figs S6E-F and S7A and Video 1). A similar pattern was observed when the mBEC were grown as a 2D monoculture (Fig. S7B and Video 2).

Supplementary video related to this article can be found at https://doi.org/10.1016/j.jhep.2024.06.002

Next, we tested the functional effects of PC ablation in BEC. Previous studies have shown the regenerative properties of BEC after their transplantation in murine models of biliary disease.[30,48] To determine if the engraftment and pro-reparative capacities of BEC were intact after PC depletion, we transplanted PC-depleted and PC-competent BEC into mice following hepatic IRI.[30]

To trace the cells, we transduced the *K19CreER^T Kif3a$^{fl/fl}$* organoids with GFP and induced PC depletion via 4OHT. Then we transplanted GFP-positive PC depleted (PC-/-). or PC-competent (PC+/+) BEC after IRI, and waited 10 days for engraftment (Fig. 2E). BEC with intact PC (PC+/+) displayed higher engraftment rates compared to those without PC (PC-/-) 10 days after transplantation (Fig. 2F,G). Moreover, PC-/- BEC do not appear to proliferate (Fig. 2H), suggesting that targeted elimination of PC in BEC inhibits the ability of the cells to engraft, proliferate, and repair the biliary compartment.

To better understand this phenotype, we performed RNA sequencing of the PC-/- and PC+/+ BEC in the *K19CreER^T Kif3a$^{fl/fl}$* organoid system. Differential expression analysis revealed that PC-ablated BEC showed significant changes in the expression of known PC markers, including downregulation of *Kif3a*, *Smo*, and *Wdr35,* among others (Fig. S8A). This analysis confirms that the expression of genes linked to the structure and function of PC is downregulated following PC depletion.

PC-depleted BEC exhibit a distinct expression profile characterised by a significant upregulation of factors associated with DNA damage response (*Atm*, *Rad52*, *Trp53bp1*), cellular senescence and senescence-associated secretory phenotype (SASP: *Mdm2*, *Il1a*, *Ccl20*, *Pdgfβ*, *Cdkn1a*, *Cdkn2b*, *Pten*, *Rb1*), as well as a significant downregulation of apoptotic (*Casp3*, *Casp8*, *Bax*, *Bad*) and proliferation markers (*Pcna*, *Ccnd1*, *Ccne1*) (Fig. 2I and Supplementary excel 1). Alongside cellular senescence, we observed morphological and functional changes (Fig. S8B). Further analysis reveals downregulation of key components of bile acid metabolism (*e.g. Prdc5, Gc, Abcd3* (Fig. S8C)) and the bile acid biosynthetic process (*e.g. Fgfr4, Sirt1, Prox1* (Fig. S8D)). Cellular senescence and SASP involvement were also confirmed (Fig. S8E).

PC-depleted BEC also have altered expression of pathways that are crucial in maintaining cell polarity (*Wdr1, ParvB, Fblim1, Msn, Myl12b*), cytoskeleton organisation (Rho family of GTPases; *e.g.*, *Rac1, Rac3, Cdc42, Rhoa, Rhob*), cell shape, motility and adhesion (*e.g.*, *Crkm, Tpm1,* Semaphorin family) (Fig. S8F).

Next, we explored *in vitro* the morphological changes observed at the transcriptomic level. PC-depleted BEC exhibit significantly increased *EpCAM* and *Sox9*, whilst decreasing the expression of functional markers such as aquaporin 1 (Fig. S9A). PC ablation in BEC led to impaired motility (Fig. S9B-D), as observed by the lack of displacement in the presence of positive stimuli. PC-depleted BEC also exhibit significantly lower rhodamine 123 efflux in comparison with PC-competent BEC (Fig. S10), suggesting decreased function of the multidrug resistance protein 1 biliary transporter.

Absence of proliferation in PC-depleted BEC (+4OHT) was confirmed by an EdU assay in our *in vitro* culture (Fig. 2J–K). Alongside this decreased proliferation, we observed a significant increase in SA-β-Gal, γH2A.X, and 53BP1 (Fig 2L and Fig. S11), all highly suggestive of DNA damage and cellular senescence.[64,65]

Cellular senescence is an essentially irreversible cell cycle arrest, induced by stressful stimuli (*e.g.*, DNA damage response[64]), and accompanied by a SASP that communicates the status of the cell to the surrounding cells.[34,65] In BEC, senescence has been shown to aggravate biliary disease[28,66–68] and impede biliary regeneration.[16]

We also assessed the effects of PC ablation in other areas of the biliary tract. Recombination in our *K19CreER^T Kif3a$^{fl/fl}$* model takes place at intra and extrahepatic level[28,30] (Fig. S12A). We injected the mice with three doses of tamoxifen to deplete the PC in the K19-positive BEC and administered 2 weeks of dietary damage, which we previously found reproduces some of the traits of BC.[16] Then we isolated IHBD, EHBD (*i.e.* common bile duct) and GB BEC from our *K19-CreER^T Kif3a$^{fl/fl}$* model (Fig. S12A).

In PC-competent BEC, we found significant differences in K19 and albumin between IHBD and EHBD. Similarly, we found significant differences in HNF4α (*Hnf4a*) between IHBD and GB regions. We also found expression differences between PC-competent and PC-depleted BEC in specific areas that were not present in other areas (*e.g.*, *Epcam* and *Tgfb1* are significantly increased in IHBD but not in EHBD or GB) (Fig. S12A).

We also stained the deep peribiliary glands in human sections to understand the involvement of PC in extrahepatic areas (Fig. S12B). We observed significantly shorter PC in the deep peribiliary glands in livers with more than 8 h of cold ischemia (Fig. S12C).

Altogether, these data suggest a complex scenario in which PC function (and the consequences of their depletion) depend on and/or contribute to the heterogeneity of the biliary tract.

PC-depleted BEC implement cellular senescence and undergo morphological/functional changes that alter their metabolic, motility and adhesion capacities, which may account for the observations found in BC.

Exploring the association between hypoxia, primary cilia loss and cellular senescence in BEC

Hypoxia has a profound effect on PC organisation, structure and maintenance (see Fig. 1). In turn, PC ablation indues cellular senescence (see Fig. 2). Therefore, to explore the connection between these three factors in greater detail, we performed a pathway focused gene expression analysis.

PC-depleted BEC (PC-/-) display significant upregulation of factors that are crucial to initiate a hypoxic response (*e.g. Hif1a*, *Hk2* and *Vegfa*) in comparison with PC-competent (PC+/+) BEC (Fig. 3A), suggesting that elimination of PC triggers a pro-hypoxic response.

To explore the consequences of this hypoxic response, we exposed PC-competent BEC to 6 h of hypoxia (0.5% O_2 at 37 °C). In these conditions, BEC increase senescence marker SA-β-Gal (Fig 3B and Fig. S13A), whilst still retaining a K19-positive phenotype (Fig. 3C). We also observed significantly decreased proliferation (Fig. 3D) and significant upregulation of p16 and p21 (Fig. S13B), all highly suggestive of the induction of senescence with hypoxic conditions. These data suggest that hypoxic conditions trigger senescence in BEC.

Next, we explored the effects of senescence on the PC. To induce senescence in PC-competent BEC *in vitro*, we administered 5 ng/ml of TGFβ as previously described.[32,33] TGFβ-induced senescence resulted in vacuolization and enlargement of BEC (Fig. S13C), decreased proliferation (Fig. S13D), and expression of p21, p27, γH2A.X and decoy receptor 2 (DCR2) (Fig. S13E). In these senescent *in vitro* conditions, the percentage of ciliated BEC significantly decreased (Fig. 3E), suggesting senescence triggers PC loss *in vitro*.

To test the effects of senescence on the PC *in vivo*, we used the *K19CreER^T Mdm2$^{fl/fl}$ TdTom^{LSL}* mouse.[28] Induction of the *K19CreER^T* recombinase, via three intraperitoneal doses of tamoxifen, results in the ablation of *Mdm2*, a key regulator of p53 (Fig. S14A). Consequently, BEC implement a p53-p21-driven cell cycle arrest that enables the determination of

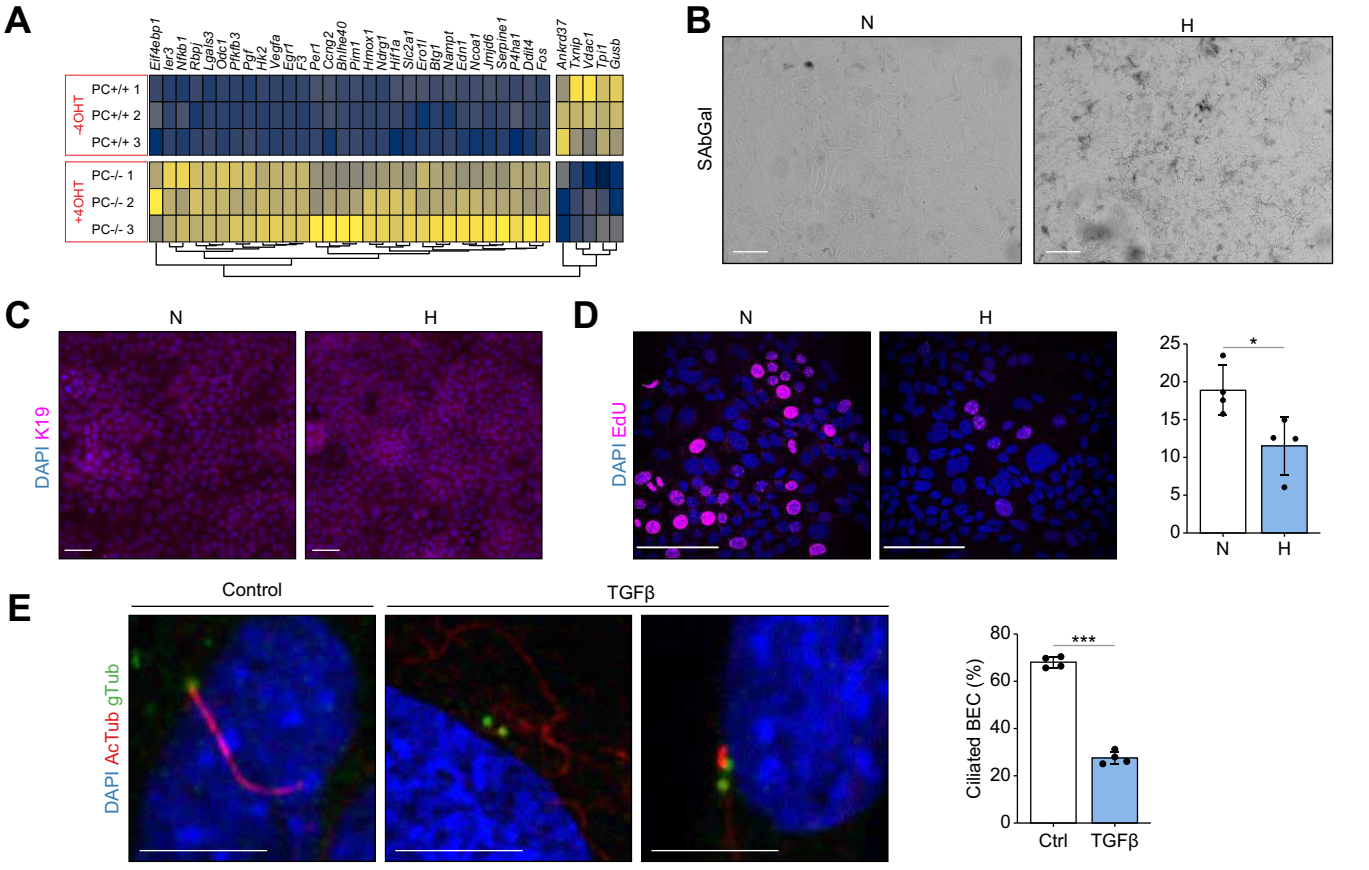

Fig. 3. Hypoxia, PC loss and senescence in BEC. (A) Heatmap of mouse hypoxia-related genes significantly differentially expressed between -4OHT (PC competent) and +4OHT (PC depleted) BEC. (B) SA-β-Gal assay in BEC in normoxia (N, 20% O_2, 5% CO_2) and hypoxia (H, 0.5% O_2 at 37 °C). SB = 100 μm. (C) Immunofluorescence of K19 in BEC subjected to 6 h of normoxia (N,) or hypoxia (H). SB = 100 μm. (D) Immunofluorescence of EdU in BEC subjected to normoxia (N) or hypoxia (H). SB = 100 μm. Right, quantification: percentage of EdU-positive BEC in normoxia (N) and hypoxia (H). n = 4 biological replicates per group. *p <0.05 (Mean ± SEM); Student's t test. (E) PC immunofluorescence: AcTub marking ciliary axoneme and γ-Tubulin (gTub) staining the basal body in TGFβ-treated (senescent) and control BEC. SB = 10 μm. Far right, quantification: percentage of ciliated BEC upon TGFβ treatment (senescence) in comparison with control BEC. n = 4 biological replicates per group. ***p <0.001 (Mean ± SEM); Student's t test. 4OHT, 4-hydroxytamoxifen; AcTub, acetylated-α-tubulin; BEC, biliary epithelial cells; EdU, 5-ethynyl-2'-deoxyuridine: gTub, γ-tubulin; H, hypoxia: N, normoxia: PC, primary cilia.

specific effects of senescence. The model also harbours a TdTom^{LSL} allowing indirect tracing of p21-positive BEC via a fluorescent reporter[28] (Fig. S14B).

Induction of this model results in significantly less ciliated BEC over the course of 21 days compared to non-induced *K19CreER^{T} Mdm2$^{fl/fl}$ TdTom^{LSL}* mice (Fig. S14C). Moreover, p21-positive TdTom^{LSL}-positive BEC had significantly less PC than their p21-negative counterparts in induced mice (Figs. S14D and E).

We also assessed the number of ciliated BEC in human primary sclerosing cholangitis and primary biliary cholangitis, conditions characterised by senescent BEC.[28,68] In human primary sclerosing cholangitis samples, the percentage of ciliated BEC significantly decreases with senescence, assessed via DCR2 expression[16] (Figs. S14F and G). However, we found no correlation between the percentage of ciliated BEC and senescence in primary biliary cholangitis (Figs. S14H and I).

Next, we tested if the PC loss in senescent cells was restricted to BEC or also present in other cell types and other senescence inductors. We checked ciliation status in a model of oncogene-induced senescence in human fibroblasts.[34,69] This model uses IMR90 cells (human fetal lung fibroblasts) in which the RAS oncogene is fused to an oestrogen receptor (IRAS cells).

Activation of the oestrogen receptor, via administration of 4OHT, leads to RAS expression and establishment of senescence. We used the vector-IMR90 (ISTOP) cells as a control cell line.[69] *In vitro* administration of 4OHT (+4OHT) to IRAS leads to the onset of senescence, assessed by increased expression of *CDKN1A* (p21) and decreased expression of *MKI67* (Ki67) (Fig. S15A).

Senescent IRAS significantly decrease the percentage and length of PC (Figs. S15B and C). Senescent IRAS also display an increased expression of *HIF1A*, suggesting activation of hypoxic pathways (Fig. S15D).

Examination of publicly available datasets of senescence[45,46] and PC[43,47] suggests PC reorganisation with senescence onset, regardless of the stimuli for senescence.

A significant decrease in genes essential for PC maintenance (*ARL13B*, *SMO*, *IFT88*) was observed in the transcriptomic signature of senescent fibroblasts[46] (Fig. S15E). Moreover, cilia-associated genes displayed changes during the single-cell RNA sequencing time course of oncogene-induced senescence in IMR90 cells[45] (Fig. S15F).

Altogether, this suggests that senescence induces profound alterations in the transcriptomic landscape of the PC, independently of the stimulus.

Based on these results, we hypothesize that PC loss, senescence and hypoxia are interlinked and a conserved phenomenon in several cell types. These three pillars appear to be fundamental to maintain BEC homeostasis and alterations in one of these parameters sets off an imbalance that impedes BEC regeneration.

Inhibition of senescence preserves primary cilia morphology during liver ischemic injury

To further explore the functional effects of senescence in the PC, we analysed ciliation in the absence of a competent senescence response, using a *p21$^{-/-}$* mouse model in which p21-driven senescence is impaired.[70]

First, we exposed livers from the *p21$^{-/-}$* mice to 10 h of cold ischemia in our mouse DBD procurement model (Fig. 4A). We found no significant differences for PC length after 10 h of cold ischemia in bile ducts with similar diameters (Fig. 4B,C).

The *p21$^{-/-}$* mice also present significantly increased levels of BEC proliferation after cold ischemia, as assessed by the percentage of PCNA-positive BEC (Fig. 4D).

Together, these results suggest that PC ablation does not occur in mice with impaired senescence, indicating that removal of the senescence response may be a potential strategy to preserve the PC in BEC. However, this p21-knockout strategy cannot be translated to the clinic, thus alternative options for the inhibition of cellular senescence are required.

Senolytics are a class of drugs that selectively eliminate senescent cells and their detrimental SASP-driven effects. A well-characterised example is ABT-737, a small molecule that targets and inhibits BCL-2, BCL-W and BCL-XL, all members of the BCL-2 family. BCL-W and BCL-XL confer a characteristic resistance to apoptosis upon senescent cells.[71] Therefore, ABT-737 leads to senescent cell death *in vitro* and *in vivo*, as shown in senescent irradiated lungs[71] and injured livers.[16,72]

To test the effects of senolytics in the PC, we administered either ABT-737 or vehicle (DMSO) to wild-type mice via intraperitoneal injection for 7 consecutive days.[73] We then exposed the livers to 10 h of cold ischemia in our mouse DBD procurement model (Fig. 4E). Livers from mice pre-treated with ABT-737 displayed significantly longer PC (Fig. 4F) and a non-significant increase in BEC proliferation (Fig. 4G, $p = 0.0553$) compared to vehicle-treated controls.

Finally, we evaluated the effects of senolytic perfusion in human livers. Briefly, segments II and III of human livers declined for transplantation were dissected and prepared (Fig. S16A) preserving the respective portal vein branches (Fig. S16B). Portal veins were then cannulated and connected to a peristaltic pump to continuously flush the segments with senolytic or vehicle solution (Figs. S16C and D). Donor data for the livers can be found in Table S4.

We used a combination of dasatinib and quercetin,[73] an FDA-approved senolytic recently used in a first-in-human open-label pilot trial addressing idiopathic pulmonary fibrosis.[74]

During perfusion, one of the segments received a combination of dasatinib and quercetin while the other received vehicle solution (DMSO in PBS). PC appears to be better preserved in the bile ducts of the dasatinib+quercetin perfused segments, as assessed by ARL13B immunofluorescence (Fig. 4H). Moreover, assessment of PC length indicates that the segments perfused with dasatinib+quercetin had significantly longer PC in comparison with the vehicle-perfused segments (Fig 4I and Fig. S16E).

Altogether, these results suggest that prevention of senescence (either through genetic models, such as *p21$^{-/-}$*, or administration of senolytics) preserves PC length and BEC proliferative capacities in both rodent and human livers. Moreover, administration of senolytics to discarded human livers, using a proof-of-concept machine perfusion, results in improved preservation of PC length.

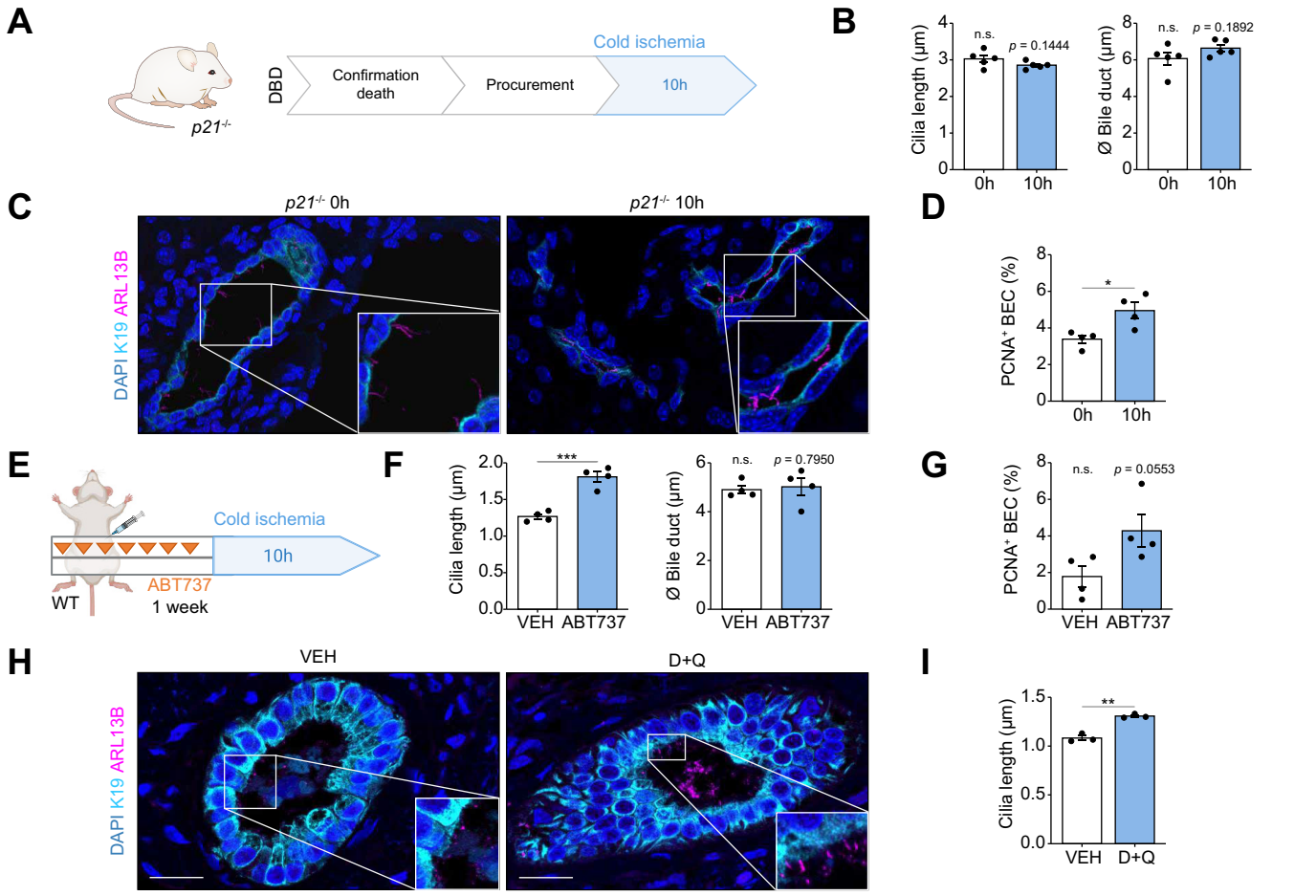

Fig. 4. Inhibition of senescence preserves PC. (A) Schematic representation of the experiment. *p21*$^{-/-}$ mice were culled following our DBD model, livers procured and subjected to 10 h of cold storage. (B) Quantification of PC length and bile duct diameter in the *p21*$^{-/-}$ livers subjected to 10 h of cold storage (n = 5 per group), Student's *t* test. (C) Immunofluorescence for K19 and ARL13B (ciliary axoneme) in *p21*$^{-/-}$ mice at 0 and 10 h of cold storage. In the square: digital magnification depicting PC. SB = 50 µm. (D) Percentage of PCNA-positive proliferating BEC in the *p21*$^{-/-}$ livers at 0 and 10 h of cold storage. n = 4 per group, **p* <0.05 (Mean ± SEM); Student's *t* test. (E) Schematic representation of the experiment. WT mice received seven daily intraperitoneal doses of the senolytic ABT737 or vehicle control (DMSO). Mice were culled following our DBD model. Livers were procured and subjected to 10 h of cold storage. (F) Quantification of PC length and bile duct diameter in livers procured from vehicle- or ABT737-treated mice. For each group, livers were subjected to 10 h of cold storage after procurement. n = 4 per group, ****p* <0.001 (Mean ± SEM); Student's *t* test. (G) Percentage of PCNA-positive proliferating BEC in vehicle- or ABT737-treated mice. For each group, livers were subjected to 10 h of cold storage after procurement. n = 4 per group, **p* <0.05 (Mean ± SEM); Student's *t* test. (H) Immunofluorescence for K19 and ARL13B (ciliary axoneme) in discarded donor human livers after vehicle or senolytic (D+Q) perfusion. In the square: digital magnification depicting PC. SB= 50 µm. (I) Quantification of PC length in discarded donor human livers after vehicle or senolytic (D+Q) perfusion (n = 3 livers). ***p* <0.01 (Mean ± SEM); Student's *t* test. BEC, biliary epithelial cells; D, dasatinib; DBD, donation after brain death; Q, quercetin; PC, primary cilia: VEH, vehicle: WT, wild-type.

Primary cilia stabilisation improves biliary anatomy following cold storage

Since senescence inhibition has a positive impact on BEC proliferation and preservation of the PC, we evaluated the reverse approach: does cilia stabilisation impact BEC regeneration and senescence in our mouse model of cold storage?

Tubastatin A is a selective inhibitor of histone deacetylase 6 (HDAC6), an enzyme that is required to disassemble the PC of the cell to allow for mitosis.[75] While overexpression of HDAC6 in BEC induces deciliation,[76] HDAC6 inhibition (via Tubastatin A) has been shown to restore PC, increase AcTub expression and downregulate Hedgehog and MAPK signaling pathways.[76]

In our experimental setting, Tubastatin A addition to BEC *in vitro* increased the protein levels of AcTub in comparison with DMSO (vehicle)-treated BEC (Fig. S17A), indicating PC stabilisation *in vitro*.[76]

Next, we perfused livers from wild-type mice with UW preservation solution supplemented with either Tubastatin A or DMSO (vehicle). Livers were procured and cold stored for 10 h in the supplemented UW solution. Bile ducts were subsequently isolated and cultured as organoids for 4 days to assess their growth rate (Fig. S17B). Bile ducts isolated from the Tubastatin A-treated livers displayed significantly increased growth rates in comparison with those isolated from the DMSO-treated ones (Fig. 5A,B and Fig. S17C).

To evaluate the functional effects of PC stabilisation on BEC *in vivo*, we administered 10 mg/kg of Tubastatin A or DMSO-vehicle to wild-type mice via intraperitoneal injection and induced hepatic injury using a well-established model of hepatic IRI (Fig. S18A). This model allowed us to simulate the undersupply of blood that occurs during organ storage, followed by restoration of perfusion and concomitant re-oxygenation

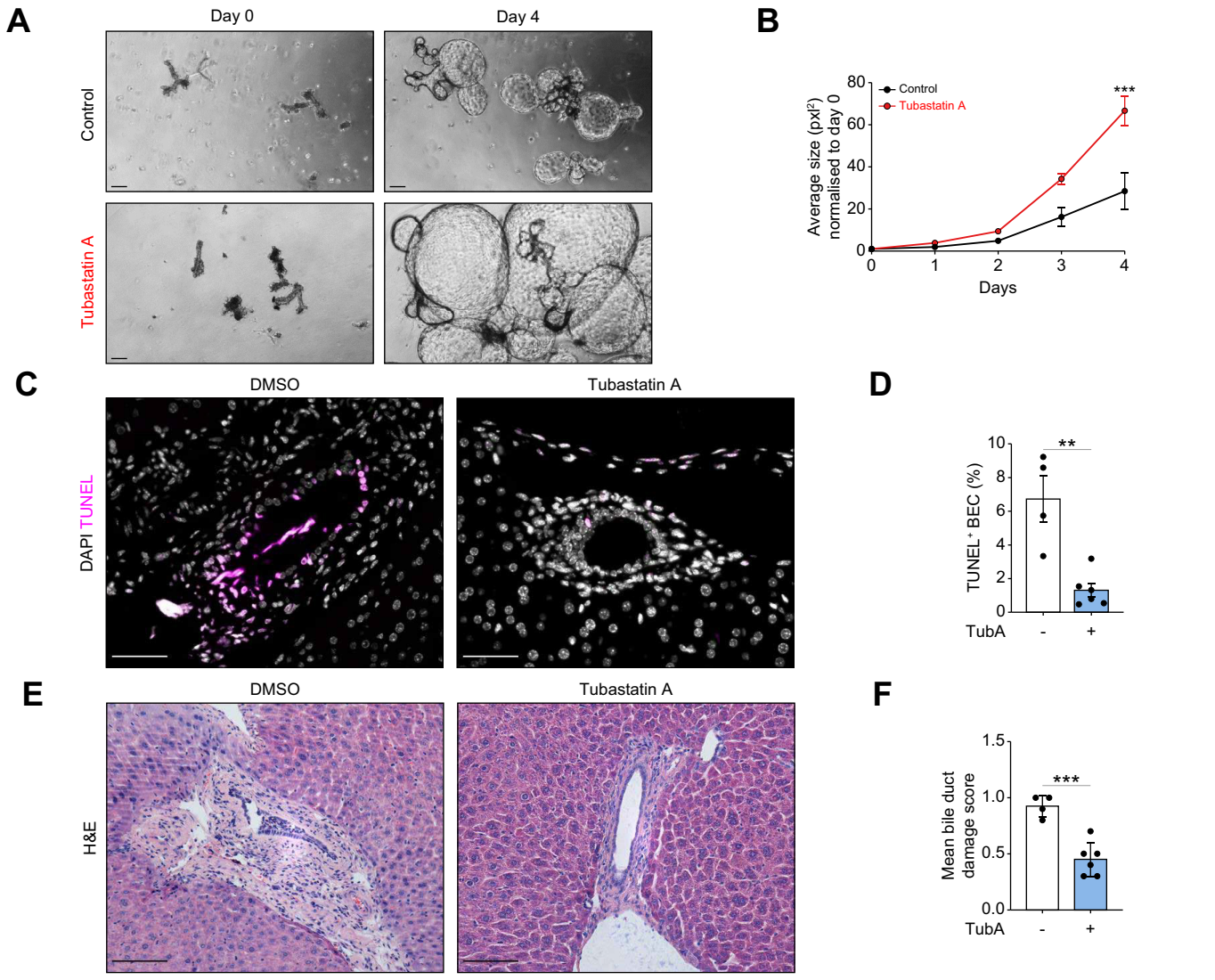

Fig. 5. PC stabilisation improves biliary anatomy following cold storage. (A) Representative brightfield images of bile ducts grown as organoids. Bile ducts were isolated from mouse livers perfused with either Tubastatin A or DMSO control, and maintained for 10 h in cold storage. Images were taken immediately after isolation (day 0) and at day 4 post-isolation. SB = 100 μm. (B) Quantification of the average organoid size (pxl^2) grown from bile ducts isolated from mouse livers perfused with DMSO control or Tubastatin A (in red), and maintained for 10 h in cold storage. ***p <0.001 (mean ± SEM), Student's t test for Day 4 (n = 4 mice each with 3 technical replicates in culture). (C) TUNEL immunofluorescence in DMSO (control)-treated compared with Tubastatin A-treated mice subjected to IRI. SB = 50 μm. (D) Quantification of TUNEL-positive BEC in DMSO (control)-treated compared with Tubastatin A-treated mice subjected to IRI. **p <0.01 (mean ± SEM), Student's t test. (E) Representative H&E images in DMSO (control)-treated compared with Tubastatin A-treated mice subjected to IRI. SB = 100 μm. (F) Integrity of bile ducts was assessed using a bile duct damage score (see Fig. S18F). A total of 10 bile ducts were scored per mouse in a range from 0 to 4. ***p <0.001 (mean ± SEM), Student's t test. BEC, biliary epithelial cells: IRI, ischemia reperfusion injury: PC, primary cilia: TubA, Tubastatin A.

(reperfusion).[29] Briefly, we clamped the hepatic artery, portal vein and common bile duct of the mouse for 30 min, removed the clamp and evaluated the mice after 24 or 48 h of reperfusion.

No significant changes in body weight or liver/body weight ratio were observed 24 h after the ischemic insult (Fig. S18B). We observed a significant reduction of AST and a trend towards lower bilirubin levels in Tubastatin A-treated mice in comparison with vehicle controls (Fig. S18C, p = 0.0978).

Upon quantification, no significant differences were found for BEC proliferation (assessed via PCNA), senescence (DCR2) or DNA damage response (γH2A.X) in mice treated with Tubastatin A in comparison with vehicle control mice at 48 h of reperfusion (Fig. S18D). Evaluation of proliferation, senescence and DNA damage response in hepatocytes also showed no significant differences (Fig. S18E).

We observed a significant decrease in TUNEL-positive BEC in Tubastatin A-treated livers compared to vehicle-treated livers (Fig. 5C,D), suggesting that PC preservation has a positive effect on BEC apoptotic rate. Moreover, evaluation of bile duct morphology revealed that Tubastatin A-treated livers displayed less biliary damage in comparison with control livers (Fig 5E,F and Fig. S18F). Our bile duct damage score (Fig. S18F) indicates that livers treated with Tubastatin A display significantly fewer defects in the BEC lining than DMSO-treated livers.

Together, these data suggest that PC-targeted strategies do not reduce cellular senescence in BEC nor increase BEC

proliferative potential. However, PC stabilisation appears to preserve bile duct morphology and prevent BEC apoptosis, suggesting a potential alternative therapeutic approach.

Discussion

BC are often referred to as the "Achilles' heel" of liver transplantation since they constitute a major factor influencing long-term graft and patient survival.[2,3] BC develop in 15-25% of all liver transplant recipients and can have a profound impact on patient's morbidity and mortality. Treatment-resistant BC frequently require re-transplantation[8] with repetitive hospital stays and additional interventions resulting in a significant care and cost burden.[7] Multiple molecular mechanisms have been suggested as a primary cause of BC, including bile-induced damage[13] and IRI.[12,14,15] However, to date, none of these mechanisms have translated into a clinical therapy capable of reducing current BC rates.

The term BC encompasses a plethora of conditions with a common target: BEC. BEC are cuboid, ciliated cells: each BEC has a primary cilium that points to the lumen of the intra- and extrahepatic biliary tree.[17]

Although PC were first described more than a century ago,[77] until very recently they had been considered vestigial organelles with no observable function. PC are nonetheless far more widespread than motile cilia and numerous studies have highlighted their importance in homeostasis and disease.[78] These solitary structures have a prominent role as mechanoreceptors responding to flow movements, chemoreceptors and detectors of light, temperature and osmolarity.[78]

PC have been shown to be essential for fibroblast migration,[79] vertebrate development[80] and to coordinate the transmission of specific extracellular signals to the interior of the cell (*e.g.*, via Hedgehog, platelet-derived growth factor, TGFβ and Wnt pathways).[81–83]

However, in the liver, little is known about the role of the PC in BEC. Biliary PC have recently been shown to act as chemosensors by detecting biliary nucleotides via P2Y12 receptors,[84] to detect changes in bile flow via Ca^{2+} and cAMP signaling[20] and to determine cell proliferation through biliary exosomes.[85]

In this study, we aimed to characterise the role of the PC in the context of liver transplantation and BC development, to understand the functional role of PC changes in the biliary tract.

In our experimental setting, we observed that liver grafts that developed BC displayed a decreased PC length in BEC pre-operatively. As cold storage is characterised by an ischemic reduction of blood supply to tissues and hypoxia,[55] we also observed that this shortening of PC correlates with the duration of ischemia both in human and murine livers. Together, these results suggest that shortened PC in BEC correspond with post-operative BC development and may be exacerbated under hypoxic cold storage conditions.

Shortening of PC in the context of hypoxia has previously been described in other cell types: murine bone marrow-derived mesenchymal stem cells cultured in hypoxic conditions lose their PC in a time-dependent manner;[86] hypoxia also inhibits PC formation in rat tail tendon fascicles, reducing cell-mediated contraction;[87] renal tubular cells subjected to ischemia shorten their PC and increase creatinine levels, indicating impaired kidney function.[88,89] Interestingly, loss of PC in renal tubular cells also resulted in increased epithelial to mesenchymal transition, a maladaptive repair to injury that can potentially result in fibrosis and chronic kidney disease ref.[90] These results indicate that in the kidneys, similar to our observations in the liver, ischemia may trigger loss of PC and a maladaptive repair response, potentially responsible for the development of postoperative complications.

To understand the functional consequences of PC loss in BEC, we used a model of conditional PC ablation: the *K19CreER^{T} Kif3a$^{fl/fl}$* mouse. In this animal model, conditional deletion of *Kif3a* (a crucial factor for the maintenance of the intraflagellar transport machinery) in K19-positive BEC causes BEC-specific, time-dependent PC loss. Using this model, we found that PC ablation in BEC both *in vitro* and *in vivo* induces cellular senescence, an essentially irreversible cell cycle arrest that profoundly impairs regeneration.[65]

PC loss appears to lead to cellular senescence in BEC and, correspondingly, senescent BEC display altered PC compared to non-senescent BEC. This phenotype appears to be conserved across different cell types and species: senescent human IMR90 fibroblasts (where senescence can be induced via ectopic expression of the RAS oncogene[69]) also present altered PC morphology; PC-depleted human fibroblasts appear to adopt a senescent phenotype,[91] and PC alterations can also be found in the transcriptomic signature of senescent fibroblasts,[46] endothelial cells, keratinocytes, melanocytes and astrocytes.[45,92] Moreover, biliary atresia – a pediatric disease characterised by ductopenia and progressive cholangiopathy – is characterised by PC abnormalities and increased cellular senescence.[27,93–95]

Our results suggest that inhibition of senescence preserves PC and proliferation of BEC. BEC in the *p21$^{-/-}$* mouse model (in which senescence is impaired[70]) maintain their PC after cold storage. The conservation of the PC structure during ischemia in the absence of senescence is highly indicative of senescence negatively impacting on PC.

Similarly, inhibition of the senescent response via pharmacological reagents (senolytics) also results in preserved PC structure in BEC. This suggests that senescence inhibition may represent a feasible strategy for the preservation of the PC and maintenance of the inherent regenerative properties of BEC. Use of senolytics also represents a more clinically relevant context as both systemic and donor liver application seems plausible.[73]

It is also possible that after senolytic treatment, the observed intact PC belong to the remaining healthy BEC and not to the cells that have been targeted by the senolytics. However, given that the inhibition of the pathways that initially lead to senescence (as in the *p21$^{-/-}$* model) results in longer PC, we suggest that inhibition of senescence is preserving the PC structure in BEC.

PC stabilisation using Tubastatin A does not appear to modify the senescent phenotype in BEC. This suggests that the chain of events in BC starts with an ischemic insult, resulting in PC loss in BEC. This induces cellular senescence and significantly reduces their ability to proliferate and repair the damage. In this sequence, targeted interventions towards senescence appear to preserve the PC and partially reverse the damage, but also suggest alternative mechanisms for senescence implementation after PC loss.

In summary, PC stabilisation appears to preserve bile duct morphology and prevent BEC apoptosis, suggesting that this may be (either alone or in combination with senolytics) a

potential approach for future therapeutics in BC. Our study showcases an interplay between ischemia, PC and senescence in BEC, indicating the importance of these mechanisms for the maintenance of homeostasis and regeneration in the biliary compartment. Our findings may help to identify alternative avenues for the treatment of BC.

Affiliations

[1]*MRC Centre for Regenerative Medicine, University of Edinburgh, 5 Little France Drive, Edinburgh, EH16 4UU, UK;* [2]*Department of Visceral, Transplant and Thoracic Surgery, OrganLife Laboratory, Centre of Operative Medicine, Innsbruck Medical University. Anichstrasse 35, 6020 Innsbruck, Austria;* [3]*MRC Human Genetics Unit, Institute of Genetics and Cancer, University of Edinburgh; Edinburgh EH4 2XU, UK;* [4]*Centre for Inflammation Research (CIR), University of Edinburgh. The Queen's Medical Research Institute, 47 Little France Crescent, Edinburgh EH16 4TJ, UK;* [5]*Edinburgh Transplant Centre, Royal Infirmary of Edinburgh; 51 Little France Crescent, Edinburgh EH16 4SA, UK;* [6]*Division of Transplantation, CLINTEC, Karolinska Institutet, 171 77 Stockholm, Sweden*

Abbreviations

4OHT, 4-hydroxytamoxifen; AcTub, acetylated-α-tubulin; AS, anastomotic stricture; AST, aspartate aminotransferase; BC, biliary complications; BEC, biliary epithelial cells; CIT, cold ischemic time; D, dasatinib; DBD, donation after brain death; DCD, donation after cardiac death; DCR2, decoy receptor 2; DDC, 3,5-diethoxycarbonyl-1,4-dihydrocollidine; EdU, 5-ethynyl-2'-deoxyuridine; EHBD, extrahepatic bile duct; gTub, γ-tubulin; GB, gallbladder; H, hypoxia; hBEC, human BEC; HDAC6, histone deacetylase 6; IHBD, intrahepatic bile duct; IRI, ischemia reperfusion injury; K19, keratin 19; mBEC, murine BEC; N, normoxia; NAS, non-anastomotic stricture; PC, primary cilia; Q, quercetin; SA-β-Gal, SA-β-galactosidase; SASP, senescence-associated secretory phenotype; scRNA-seq, single-cell RNA sequencing; TGFβ, transforming growth factor-β; TM, tamoxifen; TubA, Tubastatin A; UW, Universal Wisconsin; VEH, vehicle; WIT, warm ischemic time; WT, wild type.

Financial support

This work was supported by the UK Medical Research Council (MRC) (MR/K017047/1), the Computational and Chemical Biology of Stem Cell Niche (MR/L012766/1), the UK Regenerative Medicine Platform (MR/K026666/1) and Scottish Enterprise High Growth Spin-Out programme (PS7305102C). HE was supported by an ESOT transplant fellowship (2019) and a MRC Clinical Research Training Fellowship (MR/T029161/1).

Conflict of interest

The authors declare no competing interests.

Please refer to the accompanying ICMJE disclosure forms for further details.

Authors' contributions

Conceptualization and design (SFG, SJF), Data generation (HE, AMK, TYM, RA, MLB, SFG); Data analysis and interpretation (HE, AMK, LB, GCO, SW, SS, SFG, SJF); Manuscript preparation (HE, SFG); Review and editing (AMK, DRT, SFG); Funding acquisition (SFG, SJF).

Data availability statement

The RNA-seq data associated with this study has been deposited in NCBI Gene Expression Omnibus (SuperSeries accession number GSE220722).

Supplementary data

Supplementary data to this article can be found online at https://doi.org/10.1016/j.jhep.2024.06.002.

References

Author names in bold designate shared co-first authorship

[1] Devarbhavi H, Asrani SK, Arab JP, et al. Global burden of liver disease: 2023 update. J Hepatol 2023;79:516–537.

[2] Foley DP, Fernandez LA, Leverson G, et al. Biliary complications after liver transplantation from donation after cardiac death donors: an analysis of risk factors and long-term outcomes from a single center. Ann Surg 2011;253:817–825.

[3] O'Neill S, Roebuck A, Khoo E, et al. A meta-analysis and meta-regression of outcomes including biliary complications in donation after cardiac death liver transplantation. Transpl Int 2014;27:1159–1174.

[4] Nemes B, Gámán G, Doros A. Biliary complications after liver transplantation. Expert Rev Gastroenterol Hepatol 2015;9:447–466.

[5] Senter-Zapata M, Khan AS, Subramanian T, et al. Patient and graft survival: biliary complications after liver transplantation. J Am Coll Surgeons 2018;226:484–494.

[6] Op den Dries S, Sutton ME, Lisman T, et al. Protection of bile ducts in liver transplantation: looking beyond ischemia. Transplantation 2011;92:373–379.

[7] **Skaro AI**, **Jay CL**, Baker TB, et al. The impact of ischemic cholangiopathy in liver transplantation using donors after cardiac death: the untold story. Surgery 2009;146:543–552. discussion 52-3.

[8] Jay CL, Lyuksemburg V, Kang R, et al. The increased costs of donation after cardiac death liver transplantation: caveat emptor. Ann Surg 2010;251:743–748.

[9] Noack K, Bronk SF, Kato A, et al. The greater vulnerability of bile duct cells to reoxygenation injury than to anoxia. Implications for the pathogenesis of biliary strictures after liver transplantation. Transplantation 1993;56:495–500.

[10] Hansen T, Hollemann D, Pitton MB, et al. Histological examination and evaluation of donor bile ducts received during orthotopic liver transplantation–a morphological clue to ischemic-type biliary lesion? Virchows Arch 2012;461:41–48.

[11] Brunner SM, Junger H, Ruemmele P, et al. Bile duct damage after cold storage of deceased donor livers predicts biliary complications after liver transplantation. J Hepatol 2013;58:1133–1139.

[12] op den Dries S, Westerkamp AC, Karimian N, et al. Injury to peribiliary glands and vascular plexus before liver transplantation predicts formation of non-anastomotic biliary strictures. J Hepatol 2014;60:1172–1179.

[13] Yska MJ, Buis CI, Monbaliu D, et al. The role of bile salt toxicity in the pathogenesis of bile duct injury after non-heart-beating porcine liver transplantation. Transplantation 2008;85:1625–1631.

[14] **de Jong IEM**, **Matton APM**, van Praagh JB, et al. Peribiliary glands are key in regeneration of the human biliary epithelium after severe bile duct injury. Hepatology 2019;69(4):1719–1734.

[15] de Jong IEM, Overi D, Carpino G, et al. Persistent biliary hypoxia and lack of regeneration are key mechanisms in the pathogenesis of posttransplant nonanastomotic strictures. Hepatology 2022;75(4):814–830.

[16] Ferreira-Gonzalez S, Man TY, Esser H, et al. Senolytic treatment preserves biliary regenerative capacity lost through cellular senescence during cold storage. Sci Transl Med 2022;14:eabj4375.

[17] Huang BQ, Masyuk TV, Muff MA, et al. Isolation and characterization of cholangiocyte primary cilia. Am J Physiol Gastrointest Liver Physiol 2006;291:G500–G509.

[18] Grzelak CA, Martelotto LG, Sigglekow ND, et al. The intrahepatic signalling niche of hedgehog is defined by primary cilia positive cells during chronic liver injury. J Hepatol 2014;60:143–151.

[19] **Nauli SM**, Alenghat FJ, **Luo Y**, et al. Polycystins 1 and 2 mediate mechanosensation in the primary cilium of kidney cells. Nat Genet 2003;33:129–137.

[20] Masyuk AI, Masyuk TV, Splinter PL, et al. Cholangiocyte cilia detect changes in luminal fluid flow and transmit them into intracellular Ca2+ and camp signaling. Gastroenterology 2006;131:911–920.

[21] Gradilone SA, Masyuk AI, Splinter PL, et al. Cholangiocyte cilia express Trpv4 and detect changes in luminal tonicity inducing bicarbonate secretion. Proc Natl Acad Sci U S A. 2007;104:19138–19143.

[22] Sicklick JK, Li Y-X, Melhem A, et al. Hedgehog signaling maintains resident hepatic progenitors throughout life. Am J Physiology-Gastrointestinal Liver Physiol 2006;290:G859–G870.

[23] Kim J, Kato M, Beachy PA. Gli2 trafficking links hedgehog-dependent activation of smoothened in the primary cilium to transcriptional activation in the nucleus. Proc Natl Acad Sci USA 2009;106:21666–21671.

[24] Omenetti A, Yang L, Li Y-X, et al. Hedgehog-mediated mesenchymal–epithelial interactions modulate hepatic response to bile duct ligation. Lab Invest 2007;87:499–514.

[25] Omenetti A, Popov Y, Jung Y, et al. The Hedgehog pathway regulates remodelling responses to biliary obstruction in rats. Gut 2008;57:1275–1282.

[26] Masyuk AI, Masyuk TV, LaRusso NF. Cholangiocyte primary cilia in liver health and disease. Developmental Dyn 2008;237:2007–2012.

[27] Karjoo S, Hand NJ, Loarca L, et al. Extrahepatic cholangiocyte cilia are abnormal in biliary atresia. J Pediatr Gastroenterol Nutr 2013;57:96–101.

[28] Ferreira-Gonzalez S, Lu WY, Raven A, et al. Paracrine cellular senescence exacerbates biliary injury and impairs regeneration. Nat Commun 2018;9:1020.
[29] Abe Y, Hines IN, Zibari G, et al. Mouse model of liver ischemia and reperfusion injury: method for studying reactive oxygen and nitrogen metabolites in vivo. Free Radic Biol Med 2009;46:1–7.
[30] **Hallett JM**, **Ferreira-Gonzalez S**, Man TY, et al. Human biliary epithelial cells from discarded donor livers rescue bile duct structure and function in a mouse model of biliary disease. Cell Stem Cell 2022;29:355. 71.e10.
[31] **Ford MJ**, **Yeyati PL**, Mali GR, et al. A cell/cilia cycle biosensor for single-cell kinetics reveals persistence of cilia after G1/S transition is a general property in cells and mice. Dev Cell 2018;47:509. 23.e5.
[32] Senturk S, Mumcuoglu M, Gursoy-Yuzugullu O, et al. Transforming growth factor-beta induces senescence in hepatocellular carcinoma cells and inhibits tumor growth. Hepatology 2010;52:966–974.
[33] **Lyu G**, **Guan Y**, Zhang C, et al. Tgf-B signaling alters H4k20me3 status via Mir-29 and contributes to cellular senescence and cardiac aging. Nat Commun 2018;9:2560.
[34] **Acosta JC**, **Banito A**, Wuestefeld T, et al. A complex secretory program orchestrated by the inflammasome controls paracrine senescence. Nat Cell Biol 2013;15:978–990.
[35] Spix JK, Chay EY, Block ER, et al. Hepatocyte growth factor induces epithelial cell motility through transactivation of the epidermal growth factor receptor. Exp Cell Res 2007;313:3319–3325.
[36] Schindelin J, Arganda-Carreras I, Frise E, et al. Fiji: an open-source platform for biological-image analysis. Nat Methods 2012;9:676–682.
[37] **Kiesel P**, **Alvarez Viar G**, Tsoy N, et al. The molecular structure of mammalian primary cilia revealed by cryo-electron tomography. Nat Struct Mol Biol 2020;27(12):1115–1124.
[38] Ewels P, Magnusson M, Lundin S, et al. Multiqc: summarize analysis results for multiple tools and samples in a single report. Bioinformatics 2016;32:3047–3048.
[39] Martin M. Cutadapt removes adapter sequences from high-throughput sequencing reads. 2011 2011; 2011;17:3.
[40] Dobin A, Davis CA, Schlesinger F, et al. Star: ultrafast universal rna-seq aligner. Bioinformatics 2013;29:15–21.
[41] Liao Y, Smyth GK, Shi W. The R package Rsubread is easier, faster, cheaper and better for alignment and quantification of Rna sequencing reads. Nucleic Acids Res 2019;47:e47.
[42] Love MI, Huber W, Anders S. Moderated estimation of fold change and dispersion for Rna-seq data with Deseq2. Genome Biol. 2014;15:550.
[43] van Dam TJP, Wheway G, Slaats GG, et al. The syscilia gold standard (Scgsv1) of known ciliary components and its applications within a systems biology consortium. Cilia 2013;2:7.
[44] Carbon S, Ireland A, Mungall CJ, et al. Amigo: online access to ontology and annotation data. Bioinformatics 2009;25:288–289.
[45] **Teo YV**, **Rattanavirotkul N**, Olova N, et al. Notch signaling mediates secondary senescence. Cell Rep 2019;27:997–1007.e5.
[46] Hernandez-Segura A, de Jong TV, Melov S, et al. Unmasking transcriptional heterogeneity in senescent cells. Curr Biol 2017;27:2652. 60.e4.
[47] Vasquez SSV, van Dam J, Wheway G. An updated syscilia Gold standard (Scgsv2) of known ciliary genes, revealing the vast progress that has been made in the cilia research field. Mol Biol Cell 2021:mbcE21020089.
[48] Sampaziotis F, Muraro D, Tysoe OC, et al. Cholangiocyte organoids can repair bile ducts after transplantation in the human liver. Science 2021;371:839–846.
[49] **Hao Y**, **Hao S**, Andersen-Nissen E, et al. Integrated analysis of multimodal single-cell data. Cell 2021;184:3573–3587 e29.
[50] Alquicira-Hernandez J, Powell JE. Nebulosa recovers single-cell gene expression signals by kernel density estimation. Bioinformatics 2021;37:2485–2487.
[51] Dominguez-Gil B, Delmonico FL, Shaheen FA, et al. The critical pathway for deceased donation: reportable uniformity in the approach to deceased donation. Transpl Int 2011;24:373–378.
[52] Thuong M, Ruiz A, Evrard P, et al. New classification of donation after circulatory death donors definitions and terminology. Transpl Int 2016;29:749–759.
[53] Monbaliu D, Pirenne J, Talbot D. Liver transplantation using donation after cardiac death donors. J Hepatol 2012;56:474–485.
[54] **Kalisvaart M**, **de Haan JE**, Polak WG, et al. Onset of donor warm ischemia time in donation after circulatory death liver transplantation: hypotension or hypoxia? Liver Transpl 2018;24:1001–1010.
[55] Eltzschig HK, Eckle T. Ischemia and reperfusion–from mechanism to translation. Nat Med 2011;17:1391–1401.
[56] Ivan M, Kaelin Jr WG. The Egln-Hif O(2)-sensing system: multiple inputs and feedbacks. Mol Cell 2017;66:772–779.
[57] Schofield CJ, Ratcliffe PJ. Oxygen sensing by hif hydroxylases. Nat Rev Mol Cell Biol 2004;5:343–354.
[58] Premkumar DR, Adhikary G, Overholt JL, et al. Intracellular pathways linking hypoxia to activation of C-Fos and Ap-1. Adv Exp Med Biol 2000;475:101–109.
[59] Rosenbaum JL, Witman GB. Intraflagellar transport. Nat Rev Mol Cell Biol 2002;3:813–825.
[60] Ungricht R, Guibbal L, Lasbennes M-C, et al. Genome-wide screening in human kidney organoids identifies developmental and disease-related aspects of nephrogenesis. Cell Stem Cell 2022;29:160–175.e7.
[61] **Chen J**, **Cheng NC**, Boland JA, et al. Deletion of Kif3a in Ck19 positive cells leads to primary cilia loss, biliary cell proliferation and cystic liver lesions in taa-treated mice. Biochim Biophys Acta (BBA) - Mol Basis Dis 2022;1868(4):166335.
[62] Fickert P, Stöger U, Fuchsbichler A, et al. A new xenobiotic-induced mouse model of sclerosing cholangitis and biliary fibrosis. Am J Pathol 2007;171:525–536.
[63] Leclercq IA, Farrell GC, Field J, et al. Cyp2e1 and Cyp4a as Microsomal Catalysts of Lipid Peroxides in Murine Nonalcoholic Steatohepatitis. J Clin Invest 2000;105:1067–1075.
[64] Gorgoulis V, Adams PD, Alimonti A, et al. Cellular senescence: defining a path forward. Cell 2019;179:813–827.
[65] Muñoz-Espín D, Serrano M. Cellular senescence: from physiology to pathology. Nat Rev Mol Cell Biol 2014;15:482.
[66] Lunz JG, Contrucci S, Ruppert K, et al. Replicative senescence of biliary epithelial cells precedes bile duct loss in chronic liver allograft rejection: increased expression of P21waf1/Cip1 as a disease marker and the influence of immunosuppressive drugs. Am J Pathol 2001;158:1379–1390.
[67] Sasaki M, Ikeda H, Haga H, et al. Frequent cellular senescence in small bile ducts in primary biliary cirrhosis: a possible role in bile duct loss. J Pathol 2005;205:451–459.
[68] **Tabibian JH**, **O'Hara SP**, Splinter PL, et al. Cholangiocyte senescence by way of N-Ras activation is a characteristic of primary sclerosing cholangitis. Hepatology 2014;59:2263–2275.
[69] Innes AJ, Gil J. Imr90 Er:Ras: a cell model of oncogene-induced senescence. Methods Mol Biol. 2019;1896:83–92.
[70] Martín-Caballero J, Flores JM, García-Palencia P, et al. Tumor susceptibility of P21(waf1/Cip1)-deficient mice. Cancer Res 2001;61:6234–6238.
[71] Yosef R, Pilpel N, Tokarsky-Amiel R, et al. Directed elimination of senescent cells by inhibition of Bcl-W and Bcl-Xl. Nat Commun 2016;7:11190.
[72] Ritschka B, Knauer-Meyer T, Goncalves DS, et al. The senotherapeutic drug Abt-737 disrupts aberrant P21 expression to restore liver regeneration in adult mice. Genes Dev 2020;34:489–494.
[73] Childs BG, Gluscevic M, Baker DJ, et al. Senescent cells: an emerging target for diseases of ageing. Nat Rev Drug Discov 2017;16:718–735.
[74] Justice JN, Nambiar AM, Tchkonia T, et al. Senolytics in idiopathic pulmonary fibrosis: results from a first-in-human, open-label. Pilot Study EBioMedicine 2019;40:554–563.
[75] **Krishnamurthy K**, **Wang G**, Silva J, et al. Ceramide regulates atypical pkczeta/lambda-mediated cell polarity in primitive ectoderm cells. A Novel function of sphingolipids in morphogenesis. J Biol Chem. 2007;282:3379–3390.
[76] Gradilone SA, Radtke BN, Bogert PS, et al. Hdac6 inhibition restores ciliary expression and decreases tumor growth. Cancer Res. 2013;73:2259–2270.
[77] Kowalewski A. Entwickelungsgeschichte Des Amphioxus Lanceolatus: Académie impériale des sciences. 1867.
[78] **Mill P**, **Christensen ST**, Pedersen LB. Primary cilia as dynamic and diverse signalling hubs in development and disease. Nat Rev Genet 2023.
[79] Schneider L, Stock CM, Dieterich P, et al. The Na+/H+ exchanger Nhe1 is required for directional migration stimulated via Pdgfr-alpha in the primary cilium. J Cell Biol 2009;185(1):163–176.
[80] Goetz SC, Anderson KV. The primary cilium: a signalling centre during vertebrate development. Nat Rev Genet 2010;11:331–344.
[81] Christensen ST, Clement CA, Satir P, et al. Primary cilia and coordination of receptor tyrosine kinase (Rtk) signalling. J Pathol 2012;226:172–184.
[82] Huangfu D, Liu A, Rakeman AS, et al. Hedgehog signalling in the mouse requires intraflagellar transport proteins. Nature 2003;426:83–87.

[83] Clement CA, Ajbro KD, Koefoed K, et al. Tgf-beta signaling is associated with endocytosis at the pocket region of the primary cilium. Cell Rep 2013;3:1806–1814.
[84] Masyuk AI, Gradilone SA, Banales JM, et al. Cholangiocyte primary cilia are chemosensory organelles that detect biliary nucleotides via P2y12 purinergic receptors. Am J Physiol Gastrointest Liver Physiol 2008;295:G725–G734.
[85] Masyuk AI, Huang BQ, Ward CJ, et al. Biliary exosomes influence cholangiocyte regulatory mechanisms and proliferation through interaction with primary cilia. Am J Physiol Gastrointest Liver Physiol 2010;299:G990–G999.
[86] Proulx-Bonneau S, Annabi B. The primary cilium as a biomarker in the hypoxic adaptation of bone marrow-derived mesenchymal stromal cells: a role for the secreted frizzled-related proteins. Biomarker Insights 2011;6:107–118.
[87] Lavagnino M, Oslapas AN, Gardner KL, et al. Hypoxia inhibits primary cilia formation and reduces cell-mediated contraction in stress-deprived rat tail tendon fascicles. Muscles Ligaments Tendons J 2016;6:193–197.
[88] Verghese E, Weidenfeld R, Bertram JF, et al. Renal cilia display length alterations following tubular injury and are present early in epithelial repair. Nephrol Dial Transplant 2007;23:834–841.
[89] Kim JI, Kim J, Jang HS, et al. Reduction of oxidative stress during recovery accelerates normalization of primary cilia length that is altered after ischemic injury in murine kidneys. Am J Physiol Renal Physiol 2013;304:F1283–F1294.
[90] Han SJ, Jung JK, Im SS, et al. Deficiency of primary cilia in kidney epithelial cells induces epithelial to mesenchymal transition. Biochem Biophys Res Commun 2018;496:450–454.
[91] Carroll B, Nelson G, Rabanal-Ruiz Y, et al. Persistent Mtorc1 signaling in cell senescence results from defects in amino acid and growth factor sensing. J Cell Biol 2017;216:1949–1957.
[92] Casella G, Munk R, Kim KM, et al. Transcriptome signature of cellular senescence. Nucleic Acids Res 2019;47:7294–7305.
[93] Hartley JL, O'Callaghan C, Rossetti S, et al. Investigation of primary cilia in the pathogenesis of biliary atresia. J Pediatr Gastroenterol Nutr 2011;52:485–488.
[94] Chu AS, Russo PA, Wells RG. Cholangiocyte cilia are abnormal in syndromic and non-syndromic biliary atresia. Mod Pathol 2012;25:751–757.
[95] **Frassetto R**, **Parolini F**, Marceddu S, et al. Intra-hepatic bile duct primary cilia in biliary atresia: primary cilia in biliary atresia. Hepatol Res 2018;48.

Keywords: Liver transplantation; biliary complications; primary cilia.
Received 21 April 2023; received in revised form 5 May 2024; accepted 1 June 2024; available online 13 June 2024